A SPHERE IN A SECOND DEGREE POLYNOMIAL CREEPING FLOW PARALLEL TO A PLANE, IMPERMEABLE AND SLIPPING WALL

by N. GHALIA

(*Laboratory of Engineering Mathematics, Polytechnic School of Tunisia, University of Carthage.* BP 743*, La Marsa, Tunisia*)

F. FEUILLEBOIS

(*LIMSI, rue John von Neumann, Campus Universitaire d'Orsay,* Bt 508*,* 91405 *Orsay cedex, France*)

and

A. SELLIER[†]

(*LadHyX, Ecole Polytechnique, 91128 Palaiseau Cédex, France*)

[Received 4 April 2016. Revise 4 July 2016. Accepted 5 July 2016]

Summary

The motion of a solid and no-slip spherical body immersed in a Newtonian liquid near a motionless, plane and impermeable slip wall is investigated, in the creeping flow approximation, using on the wall the Navier slip boundary condition. The considered cases are as follows (i) a sphere either translating or rotating parallel to the wall in a quiescent liquid; (ii) a sphere either held fixed or freely-suspended in a modulated, linear or quadratic ambient shear flow. For each case, the velocity and pressure fields about the sphere together with the associated physical quantities whenever relevant (the force, torque, non-zero stresslet component on the sphere and its translational and angular velocities) are expressed in bipolar coordinates as infinite series, the coefficients of which are governed by an infinite linear system. This system is solved numerically by first truncating at an order depending on the relevant quantity and on the sphere location and wall slip length and then applying either a Gaussian elimination or a Thomas' algorithm for inverting a large tridiagonal matrix. Handy formulae for all key quantities are also derived as asymptotic expansions for a sphere-wall gap that is large compared with the sphere radius. The sensitivity of the computed associated normalized friction factors (force, torque, stresslet) and mobilities (translational and angular velocities) to both the sphere location and the wall slip length are then discussed.

1. Introduction

Various applications are concerned with a suspension of solid particles immersed in a Newtonian liquid flowing near a boundary. Particle-boundary hydrodynamic interactions play a key role in the macroscopic suspension flow properties (such as suspension effective viscosity, effective Brownian diffusion coefficient, average settling velocity). These interactions deeply depend upon the surface shape (whether planed or curved) and nature (whether solid or deformable, impermeable

[†]<sellier@ladhyx.polytechnique.fr>

Q. Jl Mech. Appl. Math, Vol. 69. No. 4 © The Author, 2016. Published by Oxford University Press;

Advance Access publication 18 August 2016. doi:10.1093/qjmam/hbw010

or permeable, not slipping or slipping). While the no-slip boundary condition for a viscous liquid is universally recognised as being the most relevant one, it is not applicable any more for instance for impermeable hydrophobic surfaces or impermeable surfaces with micro-scaled or nano-scaled patterns (in those cases, considering an average over the patterns). In such special cases, the no-slip condition must be replaced by another boundary condition allowing for a prescribed non-zero tangential component of the liquid velocity on the surface. It has recently been recognised in the literature (see for example (**1**) for a review) that a slip condition initially proposed by Navier (**2**) is the appropriate one. This condition takes a very simple form for a plane, motionless and impermeable solid wall Σ. Taking Cartesian coordinates (O, x, y, z) with associated unit vectors $(\mathbf{e}_x, \mathbf{e}_y, \mathbf{e}_z)$ and origin O attached to the $z = 0$ plane motionless surface, the boundary condition for the liquid velocity $\mathbf{v}$ are

$$\mathbf{v}.\mathbf{e}_x = \lambda \frac{\partial \mathbf{v}.\mathbf{e}_x}{\partial z}, \ \mathbf{v}.\mathbf{e}_y = \lambda \frac{\partial \mathbf{v}.\mathbf{e}_y}{\partial z} \quad \text{and } \mathbf{v}.\mathbf{e}_z = 0 \text{ at } \Sigma(z = 0), \tag{1}$$

where $\lambda \geq 0$ is the wall slip length and may be interpreted as the distance to which the velocity profile should be extrapolated inside the solid boundary for the velocity to vanish. It should be emphasized that (1) has been sustained by experimental investigations (**3–6**).[‡] Of course, the usual no-slip boundary condition is retrieved for $\lambda = 0$.

In a first step towards the modelling of the viscosity of a dilute suspension flowing above a solid plane slip wall, the attention may be restricted to the case of a single solid particle interacting with the wall. That is, hydrodynamic interactions between particles are ignored. Even for this more tractable case, determining the liquid flow velocity and pressure remains in general an involved task since these fields are governed by the unsteady non-linear Navier-Stokes equations. Fortunately, for a sufficiently small particle all inertial effects may be neglected and the liquid flow fulfills the quasi-steady creeping flow equations (that is the classical linear Stokes equations). Within this convenient and relevant low-Reynolds-number flow approximation, several papers have been concerned with the interaction of a solid no-slip spherical particle with a plane slip wall Σ[§]. To this framework belong the pioneering calculations of (**7–9**) for a sphere rotating or translating normal to a slip wall, using bipolar coordinates together with the lubrication technique for small gaps. The cases of a sphere either translating or rotating parallel to a slip wall in a fluid at rest and either held fixed or freely suspended near the slip wall in a linear ambient shear flow have also been addressed using bipolar coordinates in (**10–12**).

A general ambient Stokes flow (complying with the Navier condition (1) on the slip wall) that is weakly varying on the scale of the sphere-wall distance may be approximated by a Taylor expansion in the coordinates near the wall. By linearity of the Stokes equations, the flow problem then boils down to dealing with polynomial ambient Stokes flows. These problems have been solved, again in bipolar coordinates, for a no-slip wall ($\lambda = 0$) by retaining flows up to degree 2 in (**13**, **14**) or even up to degree 3 in (**15**), respectively. Note that, when approximating the ambient flow up to degree 2, the article (**13**) provides results of medium accuracy for the particle in ambient modulated shear flow and linear and quadratic shear flows. More accurate results have been later obtained in (**16**) for the linear shear flow and in (**14**) for the modulated and quadratic shear flows. The case of the quadratic shear flow near a slip wall ($\lambda > 0$) has been briefly addressed in (**17**, **18**) with also asymptotic expansions of the force, torque and non-zero stresslet component exerted on a *distant* sphere *held fixed* in the

[‡] A typical value of the slip length would be around 100 μm.

[§] Note that there is a related problem in low pressure gases at low Knudsen number, where a slip condition is applied for the gas on all surfaces. That boundary condition is equivalent to the Navier condition (1).

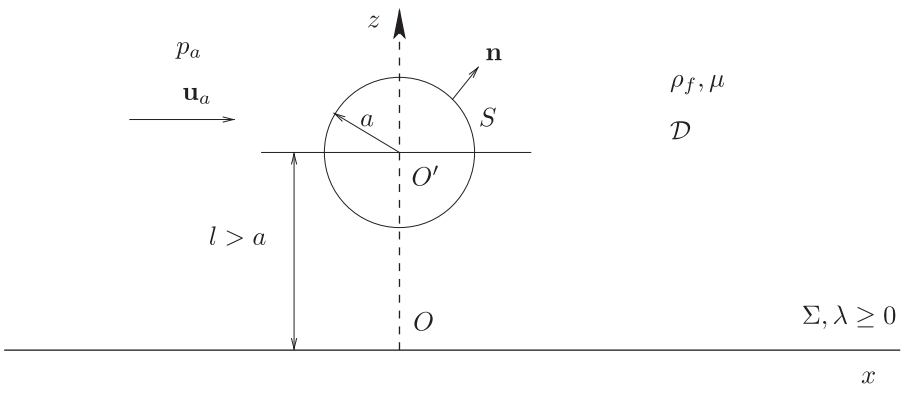

Fig. 1 A solid sphere in the vicinity of a plane, motionless, impermeable and slipping wall Σ with slip length λ

quadratic shear flow. The aim of this work is, in the framework of a sphere near a slipping wall, to provide a new solution for the modulated shear flow, to give more comprehensive results for the ambient quadratic shear flow and to provide asymptotic results for a distant sphere either translating or rotating parallel with the wall in a quiescent liquid or immersed in a linear or quadratic shear flow[‖].

The article is organized as follows. The notation and addressed second-order unidirectional ambient Stokes flow are presented in section 2 while the case of the ambient modulated shear flow is investigated in section 3 either for a close sphere or a distant one (deriving then asymptotic estimates). The treatment of the linear and quadratic ambient shear flows is handled in section 4. The coefficients in the series of the solutions in bipolar coordinates are calculated using two different methods and the numerical results for arbitrary sphere location are presented in section 5 together with the asymptotic analysis for a distant sphere. Finally, concluding remarks are in section 6.

2. Governing problems and selected ambient flow

Consider, as illustrated in Fig. 1, a solid sphere with centre O', radius a and surface S immersed in a Newtonian liquid with uniform density ρ_f and viscosity μ above a plane, motionless, impermeable and slipping wall Σ. Cartesian coordinates (O, x, y, z) with unit vectors $(\mathbf{e}_x, \mathbf{e}_y, \mathbf{e}_z)$ are attached to the wall represented by $z = 0$ and the sphere centre O' is located on the $(O, \mathbf{e}_z)$ axis with $\mathbf{OO'} = l\mathbf{e}_z$ and $l > a$.

In absence of the sphere, the ambient liquid velocity and pressure are $(\mathbf{u}_a, p_a)$ in the entire $z > 0$ half space. The solid sphere experiences a rigid-body motion described by its translational velocity $\mathbf{U}$ (that is the velocity of its centre O') and angular velocity $\mathbf{\Omega}$. Let the disturbed flow velocity and pressure in the liquid domain $\mathcal{D}$ around the particle be $(\mathbf{u}_a + \mathbf{u}, p_a + p)$, respectively. Let the scale of both velocity fields be V. Inertial effects are assumed to be negligible, that is $\mathrm{Re} = \rho_f Va/\mu \ll 1$. Under these assumptions, both ambient and disturbed flows obey the Stokes equations. With the

[‖] correcting here an error made in (**18**) for the stresslet component estimate.

appropriate boundary conditions, the governing problems read

$$\mu\nabla^2\mathbf{u}_a = \nabla p_a \quad \text{and} \quad \nabla.\mathbf{u}_a = 0 \quad \text{for} \quad z > 0, \tag{2}$$

$$\mathbf{u}_a.\mathbf{e}_z = 0, \quad \mathbf{u}_a.\mathbf{e}_x = \lambda\frac{\partial \mathbf{u}_a.\mathbf{e}_x}{\partial z} \quad \text{and} \quad \mathbf{u}_a.\mathbf{e}_y = \lambda\frac{\partial \mathbf{u}_a.\mathbf{e}_y}{\partial z} \qquad \text{on } \Sigma(z=0), \tag{3}$$

$$\mu\nabla^2\mathbf{u} = \nabla p \quad \text{and} \quad \nabla.\mathbf{u} = 0 \quad \text{in} \quad \mathcal{D}, \quad (\mathbf{u}, p) \to (\mathbf{0}, 0) \quad \text{as} \quad |\mathbf{OM}| \to \infty, \tag{4}$$

$$\mathbf{u}.\mathbf{e}_z = 0, \quad \mathbf{u}.\mathbf{e}_x = \lambda\frac{\partial \mathbf{u}.\mathbf{e}_x}{\partial z} \quad \text{and} \quad \mathbf{u}.\mathbf{e}_y = \lambda\frac{\partial \mathbf{u}.\mathbf{e}_y}{\partial z} \qquad \text{on } \Sigma(z=0), \tag{5}$$

$$\mathbf{u} = -\mathbf{u}_a + \mathbf{U} + \boldsymbol{\Omega} \wedge \mathbf{O'M} \ \text{ on } \ S, \tag{6}$$

where M denotes a current point in the flow field. Equations (3) and (5) are the mixed-type Navier slip boundary conditions (**2**) and $\lambda \geq 0$ designates the so-called wall slip length which quantifies the wall ability to let the flow slip tangent to it. As specified by (6), there is no slip on the sphere surface S.

Let $\boldsymbol{\sigma}$ be the stress tensor of the flow field $(\mathbf{u}, p)$. The flow field $(\mathbf{u}_a + \mathbf{u}, p_a + p)$ exerts on the sphere the following force $\mathbf{F}$ and torque $\mathbf{T}$ about the point O'

$$\mathbf{F} = \int_S \boldsymbol{\sigma}.\mathbf{n}dS, \quad \mathbf{T} = \int_S \mathbf{O'M} \wedge \boldsymbol{\sigma}.\mathbf{n}dS \tag{7}$$

with $\mathbf{n}$ (see Fig. 1) the unit normal on S pointing into the liquid. In practice, three different circumstances arise:

Case (1): A sphere experiencing a prescribed rigid-body motion $(\mathbf{U}, \boldsymbol{\Omega})$ in a quiescent liquid ($\mathbf{u}_a = \mathbf{0}$ and $p_a = 0$). The resulting hydrodynamic force $\mathbf{F}$ and torque $\mathbf{T}$, denoted below by $\mathbf{F}_h(\mathbf{U}, \boldsymbol{\Omega})$ and $\mathbf{T}_h(\mathbf{U}, \boldsymbol{\Omega})$, linearly depend on $\mathbf{U}$ and $\boldsymbol{\Omega}$.

Case (2): A sphere *held fixed* ($\mathbf{U} = \boldsymbol{\Omega} = \mathbf{0}$) in a given ambient Stokes flow $(\mathbf{u}_a, p_a)$ satisfying (2)-(3). In this case the resulting force and torque on the sphere, given by (7), are denoted by $\mathbf{F}_a$ and $\mathbf{T}_a$.

Case (3): A *freely suspended* sphere in the ambient flow $(\mathbf{u}_a, p_a)$. Its unknown rigid-body motion $(\mathbf{U}, \boldsymbol{\Omega})$ is then determined by requiring the sphere with negligible inertia to be force-free and torque-free. Combining by linearity the previous Cases (1) and (2), provides the relationships

$$\mathbf{F}_h(\mathbf{U}, \boldsymbol{\Omega}) = -\mathbf{F}_a, \quad \mathbf{T}_h(\mathbf{U}, \boldsymbol{\Omega}) = -\mathbf{T}_a. \tag{8}$$

Since $\mathbf{F}_h(\mathbf{U}, \boldsymbol{\Omega})$ and $\mathbf{T}_h(\mathbf{U}, \boldsymbol{\Omega})$ linearly depend upon $(\mathbf{U}, \boldsymbol{\Omega})$, the conditions (8) result in a linear system for $(\mathbf{U}, \boldsymbol{\Omega})$.

This work henceforth restricts attention to the following ambient velocity and pressure fields

$$\mathbf{u}_a = [k_\mathrm{s}(z+\lambda) + 2k_\mathrm{m}y(z+\lambda) + k_\mathrm{q}z^2]\mathbf{e}_x, \quad p_a = 2\mu k_\mathrm{q}x, \tag{9}$$

where $k_\mathrm{s}, k_\mathrm{q}$ and k_m are prescribed constants. Such a flow is the most general second-order *unidirectional* Stokes flow parallel to the slipping wall on which it satisfies the Navier slip conditions (3). Clearly, $\mathbf{u}_a$ consists of a 'pure'[¶]' shear flow $k_\mathrm{s}(z+\lambda)\mathbf{e}_x$, a 'modulated' shear flow

[¶] Due to the boundary condition (3) such a flow is actually linear in $z+\lambda$.

$2k_{\mathrm{m}}y(z+\lambda)\mathbf{e}_x$ and a quadratic shear flow $k_{\mathrm{q}}z^2\mathbf{e}_x$. By superposition, it is sufficient to successively handle those ambient flows in solving the general problem (4)–(6) and (8). As mentioned in the introduction, this has been achieved using bipolar coordinates for a no-slip wall ($\lambda = 0$) in (**16**, **14**) and for a slipping wall ($\lambda > 0$) in (**10**–**12**, **17**, **18**).

3. Sphere immersed in a modulated shear flow

This section deals with a sphere held fixed or freely suspended in the ambient velocity field $\mathbf{u}_a = 2k_{\mathrm{m}}y(z+\lambda)\mathbf{e}_x$.

3.1 *Relevant flow decomposition*

By linearity, the flow field $\mathbf{u}_a = 2k_{\mathrm{m}}y(z+\lambda)\mathbf{e}_x$ is split as the sum of a 'straining' flow $\mathbf{v}_{st}$ and a 'modulated rotational' flow $\mathbf{v}_{rot}$ with zero pressures and such that

$$2k_{\mathrm{m}}y(z+\lambda)\mathbf{e}_x = \mathbf{v}_{st} + \mathbf{v}_{rot}, \tag{10}$$

$$\mathbf{v}_{st} = k_{\mathrm{m}}(z+\lambda)[y\mathbf{e}_x + x\mathbf{e}_y], \quad \mathbf{v}_{rot} = k_{\mathrm{m}}(z+\lambda)[y\mathbf{e}_x - x\mathbf{e}_y]. \tag{11}$$

Invoking symmetries, as done in (**13**, **14**) for the $\lambda = 0$ case, easily shows that a sphere *held fixed* in the 'straining' flow $\mathbf{v}_{st}$ experiences zero force and zero torque. Hence, the 'straining' flow does not contribute to the motion of a sphere freely suspended in the ambient polynomial flow (9). It should be possible to gain the flow disturbance $(\mathbf{u}, p)$ about a sphere *held fixed* in the flow $\mathbf{v}_{st}$ for a slipping wall ($\lambda > 0$) by extending the procedure developed in (**14**) for the no-slip wall ($\lambda = 0$). However, this appears to be a lengthy task. Since it is also useless in addressing the motion of the sphere in the ambient flow (9), such an investigation is therefore not handled in the present work.

3.2 *Solution for the modulated rotational flow*

For convenience, we introduce cylindrical polar coordinates (ρ, z, ϕ) defined by $\rho = \{x^2 + y^2\}^{1/2}$, $x = \rho\cos\phi$, $y = \rho\sin\phi$ and the associated unit vectors $\mathbf{e}_\rho = \cos\phi\,\mathbf{e}_x + \sin\phi\,\mathbf{e}_y$ and $\mathbf{e}_\phi = \mathbf{e}_z \times \mathbf{e}_\rho$. Therefrom we also define the bipolar coordinates η and ξ such that (**19**)

$$\rho = \frac{c\sin\eta}{\cosh\xi - \cos\eta}, \quad z = \frac{c\sinh\xi}{\cosh\xi - \cos\eta}, \quad c = (l^2 - a^2)^{1/2}, \tag{12}$$

where $0 \le \phi \le 2\pi$, $0 \le \eta \le \pi$ and $0 \le \xi \le \alpha$ in the liquid domain $\mathcal{D}$. The domain boundaries are the $\xi = z = 0$ plane slipping wall Σ and the sphere surface S on which $\xi = \alpha$ with $\cosh\alpha = l/a$. As shown for instance in (**20**, **21**), using bipolar coordinates is quite efficient when dealing with such a liquid domain geometry. More generally, these coordinates are also convenient for deriving accurate solutions of Stokes flows whenever the bounded or unbounded liquid domain has a boundary consisting of two different spheres or of one sphere and a plane (for several related references, apart the ones quoted in this paper, the reader is directed to (**15**)).

3.2.1 Pressure and velocity disturbances. The treatment proposed in (**9**) for a sphere rotating normal to a slipping wall is extended to the present case of a sphere *held fixed* in the ambient modulated rotational flow field $\mathbf{v}_{rot}$. The flow about the sphere has a zero pressure ($p = 0$) and a

velocity $\mathbf{v}_{rot} + k_{\mathrm{m}} v(\rho, z)\mathbf{e}_\phi$ where v is an unknown function. From the general problem (4)–(6), it follows that v should satisfy

$$\left\{ \frac{\partial^2}{\partial \rho^2} + \frac{1}{\rho}\frac{\partial}{\partial \rho} + \frac{\partial^2}{\partial z^2} - \frac{1}{\rho^2} \right\} v = 0, \quad v \to 0 \text{ as } (\rho^2 + z^2)^{1/2} \to \infty, \tag{13}$$

$$v = \lambda \frac{\partial v}{\partial z} \quad \text{for } z = 0, \quad v = \rho\,(z + \lambda) \ \text{ on } S. \tag{14}$$

Invoking (**22**), the general solution of (13) may be expressed in terms of the bipolar coordinates (η, ξ) defined by (12) as follows

$$v = c^2(\cosh \xi - t)^{1/2} \sin \eta \sum_{n \geq 1} [A_n \cosh(\gamma_n \xi) + B_n \sinh(\gamma_n \xi)] P_n'(t), \tag{15}$$

where A_n and B_n are unknown coefficients vanishing for n large, $t = \cos \eta$, $\gamma_n = n + 1/2$, $P_n(t)$ denotes the Legendre polynomial of order n and the prime designates a differentiation with respect to t. Appealing to (**9**), the first boundary condition (14) on the $z = \xi = 0$ slipping plane wall becomes

$$A_n = \frac{\lambda}{c}\left\{ (n + \frac{1}{2})B_n - \frac{1}{2}(n-1)B_{n-1} - \frac{1}{2}(n+2)B_{n+1} \right\} \quad \text{for } n \geq 1. \tag{16}$$

In enforcing on the $\xi = \alpha$ sphere surface S the second boundary condition (14) it is convenient to use the following identities[#]

$$(\cosh \alpha - t)^{-3/2} = 2\sqrt{2} \sum_{n \geq 1} \mathrm{e}^{-\gamma_n \alpha} P_n'(t), \tag{17}$$

$$3 \sinh \alpha (\cosh \alpha - t)^{-5/2} = 4\sqrt{2} \sum_{n \geq 1} \gamma_n \mathrm{e}^{-\gamma_n \alpha} P_n'(t). \tag{18}$$

Requiring that $v = \rho(z + \lambda)$ for $\xi = \alpha$ then yields the relationship

$$A_n \cosh(\gamma_n \alpha) + B_n \sinh(\gamma_n \alpha) = 2\sqrt{2}\mathrm{e}^{-\gamma_n \alpha} \left[\frac{\lambda}{a \sinh \alpha} + \frac{2n+1}{3} \right] \quad \text{for } n \geq 1. \tag{19}$$

Combining (16) with (19) then provides the following infinite linear system for the unknown coefficients B_n

$$(\frac{1-n}{2})B_{n-1} + [\gamma_n + \frac{a}{\lambda} \sinh \alpha \tanh(\gamma_n \alpha)]B_n - (\frac{n+2}{2})B_{n+1} = \frac{a}{\lambda} \sinh \alpha J_n, \quad n \geq 1 \tag{20}$$

to be solved with the definitions and behaviour

$$\gamma_n = n + \frac{1}{2}, \ J_n = \frac{2\sqrt{2}\mathrm{e}^{-\gamma_n \alpha}}{\cosh(\gamma_n \alpha)} \left[\frac{\lambda}{a \sinh \alpha} + \frac{2n+1}{3} \right], \quad B_n \to 0 \text{ as } n \to \infty. \tag{21}$$

[#] The identity (17) is obtained, for instance, by differentiating the relation (2.8) given in (**23**) while (18) is immediately retrieved by differentiating (17) with respect to α.

Once (20)–(21) is solved the calculation of the velocity disturbance $k_{\rm m}v(\rho, z)\mathbf{e}_\phi$ follows from (15) and from the relationship (19)

$$A_n = J_n - B_n \tanh \gamma_n \alpha, \quad n \geq 1. \tag{22}$$

3.2.2 Torque about a fixed sphere. Angular velocity of a freely-suspended sphere. Clearly, the axisymmetric flow $k_{\rm m}v(\rho, z)\mathbf{e}_\phi$ exerts a zero force on the fixed sphere. In contrast, it applies a non-zero torque $\mathbf{C}_{mod}$ on the sphere about its centre O'. For v of the general form (15) this torque is parallel with $\mathbf{e}_z$ and given versus the coefficients A_n and B_n in (**23**). Using the link $c = a \sinh \alpha$, it reads

$$\mathbf{C}_{mod} = -4\sqrt{2}k_{\rm m}\pi\mu a^4 \sinh^4 \alpha \sum_{n\geq 1} n(n+1)[A_n + B_n]\mathbf{e}_z. \tag{23}$$

The torque $\mathbf{C}_{mod}$ on the fixed sphere depends upon the normalised slip length $\overline{\lambda} = \lambda/a$ and the normalised wall-sphere gap $l/a - 1$. For large l/a the influence of the plane wall vanishes and $\mathbf{C}_{mod}$ tends to the value $-8\pi a^3 l\mu k_{\rm m}\mathbf{e}_z$ predicted by the usual Faxen (**24**) relationship. As in (**14**), we therefore introduce the friction coefficient c^m_{zx} for the modulated shear flow (and modulated rotational flow) such that

$$\mathbf{C}_{mod} = -8\pi a^3 l\mu k_{\rm m} c^m_{zx}\mathbf{e}_z, \ c^m_{zx} = \frac{\sqrt{2}\sinh^4 \alpha}{2\cosh \alpha} \sum_{n\geq 1} n(n+1)[A_n + B_n]. \tag{24}$$

Note that analogous results were derived in (**9**) for a sphere rotating at the angular velocity $\Omega\mathbf{e}_z$ in a quiescent liquid (no ambient flow). In that case, the torque $\mathbf{C}_{rot}$ exerted on the rotating sphere is

$$\mathbf{C}_{rot} = -8\pi a^3 \mu\Omega c^r_{zz}\mathbf{e}_z, \ c^r_{zz} = \frac{\sinh^3 \alpha}{\sqrt{2}} \sum_{n\geq 1} n(n+1)[A_n + B_n], \tag{25}$$

with coefficients A_n and B_n still given by solving (20)–(22) but with J_n now given by

$$J_n = 2\sqrt{2}[1 - \tanh \gamma_n \alpha]. \tag{26}$$

Accordingly (recall (8)), a sphere that is *freely-suspended* in the modulated shear flow $2k_{\rm m}y(z + \lambda)\mathbf{e}_x$ rotates (without translating) parallel with $\mathbf{e}_z$ at the angular velocity $\Omega\mathbf{e}_z$ with

$$\Omega = -k_{\rm m} l\omega, \ \omega = c^m_{zx}/c^r_{zz}, \tag{27}$$

where ω is a normalized angular velocity.

3.3 *Numerical implementation and results*

For a no-slip wall ($\lambda = 0$) it is possible to obtain analytical solutions with $A_n = 0$ and $B_n = 2\sqrt{2}[1/\tanh(\gamma_n\alpha) - 1]$ for the rotating sphere (see (**9**)) and $B_n = 2\sqrt{2}(2n+1)[1/\tanh(\gamma_n\alpha) - 1]/3$ (with A_n given by (22)) for the sphere held fixed in the modulated rotational flow (see (**14**)).

For a slipping wall ($\lambda > 0$) a numerical treatment is needed in order to obtain the coefficients B_n which vanish as n becomes infinite (see (21)) and are solutions of the linear system (20). This linear

system is now denoted as $L(B_n) = d_n$ (with d_n the right-hand side of (20)) and let c_t be the resulting normalised torque (that is either c_{zx}^m or c_{zz}^r). Two different numerical methods were employed to compute, at a prescribed small accuracy level ϵ_l, the torque friction coefficient c_t:

(i) The technique, introduced in (**23**) for a sphere rotating near a plane surfactant layer and further employed in (**9**) for the sphere rotating normal to the slipping wall and in (**16**) for other problems involving a sphere and a no-slip wall. It consists in setting $B_n = t_n + B_1 v_n$ for $n \geq 1$ with series (t_n) and (v_n) such that $t_1 = 0, v_1 = 1, L(t_n) = d_n$ and $L(v_n) = 0$. For a prescribed truncation level $N + 1$ one first gets, by induction and from (t_1, v_1) and (20), the terms t_m and v_m for $2 \leq m \leq N$. Requiring B_n to vanish for n large (that is here for $n = N$) gives the solution $B_1 = B_1(N) := -t_N/v_N$ which then from the decomposition $B_n = t_n + B_1 v_n$ provides the coefficients $B_2, ..., B_N$ and the resulting approximation $c_t(N)$ of the friction factor. The entire procedure is iteratively repeated by increasing the value of the integer N and stopped as N reaches a convergence value N_1 which is the smallest positive integer such that $|c_t(N + 1) - c_t(N)| < \epsilon_l$ where ϵ_l is a prescribed tolerance.

(ii) The second procedure is the classical one. It consists in solving for $(B_1, ..., B_N)$ the linear $N - equation$ system obtained by setting $B_{N+1} = 0$ and using the equations (20) for $n = 1, ..., N$. The approximation of c_t is $c_t(N)$ and, as for the previous method (i), the procedure is iteratively repeated and stopped for a convergence value N_2 for which the error on c_t is less than ϵ_l.

Those two alternative methods have been coded in Fortran using double precision. They do not approximate the $B_n's$ with the same accuracy level since method (i) is explicit and method (ii) is implicit. Consequently, for a prescribed value of ϵ_l the convergence values of N_1 and N_2 are not necessarily identical. Moreover, both N_1 and N_2 also depend upon the sphere location l/a, the normalised slip length $\overline{\lambda} = \lambda/a$ and the addressed problem (rotating sphere or sphere held fixed in the modulated rotational flow).

Table **1** gives for a rotating sphere and $\epsilon_l = 10^{-7}$ the quantities N_1, N_2 and c_{zz}^r for several values of λ/a and different sphere locations $l/a = \cosh(\alpha)$. Both techniques (i) and (ii) provide identical six-digit approximations of c_{zz}^r. These results are in good agreement with the predictions obtained by the quite different boundary integral equation (BIE) approach (see this article conclusions). For instance, using 1058 collocation points on the sphere surface the (less accurate) BIE Code gives $c_{zz}^r = 1.023149$ for $\alpha = \lambda/a = 0.5$. For very small sphere to wall gaps ($l/a - 1 \ll 1$) the BIE method is not appropriate because the mesh on the sphere should be too refined. Method (ii) can be used by increasing N_2, but at some stage the size of the matrix to be inverted becomes prohibitively large for present computer memory. Then method (i) becomes more adapted because there is no such large matrix to store and invert. However, being explicit the method (i) requires a large number of digits in intermediate calculations: typically quadruple precision (32 digits), or more (using computer algebra software), is needed to ascertain the required accuracy (see for example for details (**16**) in the particular case $\lambda = 0$).

Surprisingly, the results reported in (**9**) using the above technique (i) are not in perfect agreement with our results and the BIE predictions. Note that discrepancies especially arise when both $\overline{\lambda}$ and the normalised gap $l/a - 1$ become small. It might be that those authors have used an insufficient single (eight-digit) precision in their numerical implementation, therefore obtaining results of medium accuracy. One should actually replace Table **B** of (**9**) with the present Table **2** indicating the corrected six-digit values of c_{zz}^r.

Table 1 Torque friction coefficient c^r_{zz} (recall definition (25)) for several sphere locations $l/a = \cosh(\alpha)$ and different normalised slip lengths $\overline{\lambda} = \lambda/a$. Both methods (i) and (ii), here run for $\epsilon_l = 10^{-7}$, provide the identical and reported six-digit values of c^r_{zz}. The table also displays the associated convergence integers N_1 and N_2 and in its last column (for comparison purposes) the less accurate values obtained in (**9**)

α	l/a	$\overline{\lambda}$	N_1	N_2	c^r_{zz}	(**9**)
0.1	~ 1.005	0.1	41	99	1.113946	1.097966
0.1	~ 1.005	0.5	78	99	1.026519	1.021974
0.1	~ 1.005	2.5	159	141	0.949742	0.949170
0.1	~ 1.005	5	208	177	0.930107	0.929919
0.2	~ 1.020	0.1	22	51	1.107806	1.082618
0.2	~ 1.020	0.5	41	52	1.026126	1.018354
0.2	~ 1.020	2.5	86	77	0.951907	0.950888
0.2	~ 1.020	5	114	98	0.932702	0.932365
0.5	~ 1.128	0.1	10	22	1.076332	1.052665
0.5	~ 1.128	0.5	17	22	1.023153	1.013755
0.5	~ 1.128	2.5	37	34	0.965008	0.963549
0.5	~ 1.128	5	51	44	0.948759	0.948256
1	~ 1.543	0.1	6	11	1.029249	1.024901
1	~ 1.543	0.5	9	11	1.013441	1.011094
1	~ 1.543	2.5	19	17	0.989347	0.988835
1	~ 1.543	5	25	22	0.981106	0.980910
2	~ 3.762	0.1	3	6	1.002174	1.002153
2	~ 3.762	0.5	4	6	1.001603	1.001587
2	~ 3.762	2.5	8	7	1.000183	1.000599
2	~ 3.762	5	10	9	0.999447	0.999444

As shown in Fig. 2, the torque coefficient c^r_{zz} is close to unity whatever $\overline{\lambda} \geq 0$ and $l/a \geq 1$. It also weakly either increases or decreases as l/a decays (that is as the sphere approaches the wall) when λ is either close to zero or larger than unity, respectively. Not surprisingly, for a given sphere location c^r_{zz} drops as the normalised slip length $\overline{\lambda}$ increases since the friction exerted on the flow by the wall then becomes weaker. Finally, it is remarked that $c^r_{zz} - 1$ quickly vanishes as l/a becomes large. As detailed below in Section 3.4 (see (28)), it turns out that $c^r_{zz} - 1 = O(a^3/l^3)$ for $l \gg a$.

Accurate computations of c^m_{zx} and of the normalised angular velocity ω have been also performed using both techniques (i) and (ii). Some illustrating eight-digit results (that is obtained for the accuracy level $\epsilon_l = 10^{-9}$) are listed in Table **3**.

By comparison, running the previously-mentioned BIE Code with 1058 collocation points on the sphere boundary gives $c^m_{zx} = 1.350242$ and $c^r_{zz} = 1.014215$ for $l/a - 1 = \lambda/a = 0.5$. Using superscripts m for a sphere held fixed in the modulated shear and r for the case of the rotating sphere, we also provide the number of terms for convergence N^m_1, N^r_1, N^m_2 and N^r_2 in Table **3**. As for Table **1**, these numbers are seen to strongly increase with a/l and λ/a because the flow structure which takes

Table 2 Corrected values of the torque friction factor c_{zz}^r which should replace the ones given in (**9**) (Table **2**). Like in that reference, the first column gives the ratio a/λ and the sphere location is given by the value of α with $l/a = \cosh(\alpha)$

a/λ	$\alpha = 0.1$	$\alpha = 0.2$	$\alpha = 0.5$	$\alpha = 1.0$	$\alpha = 2.0$
0.2	0.930107	0.932702	0.948759	0.981106	0.999447
0.4	0.949743	0.951907	0.965009	0.989347	1.000183
0.6	0.965216	0.966983	0.977434	0.995167	1.000609
2.0	1.026519	1.026126	1.023153	1.013441	1.001603
4.0	1.066696	1.063987	1.049484	1.021951	1.001937
6.0	1.088736	1.084741	1.062742	1.025723	1.002065
10	1.113946	1.107806	1.076332	1.029249	1.002174
40	1.161024	1.148672	1.096844	1.033939	1.002307
100	1.176726	1.161019	1.101957	1.034992	1.002335
∞	1.190962	1.170931	1.105622	1.035719	1.002353

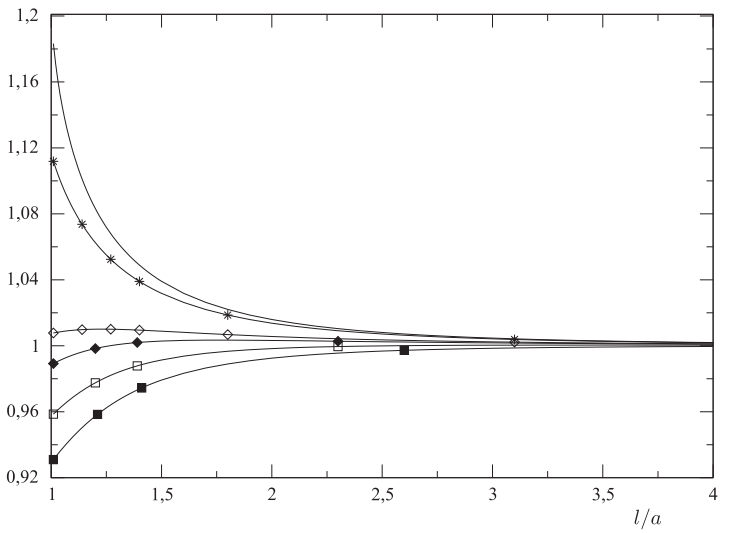

Fig. 2 Torque coefficient c_{zz}^r for a sphere rotating normal to the plane slipping wall in a quiescent liquid. $\overline{\lambda} = 0$ (solid line), $\overline{\lambda} = 0.1(*)$, $\overline{\lambda} = 0.7(\Diamond)$, $\overline{\lambda} = 1(\blacklozenge)$, $\overline{\lambda} = 2(\square)$ and $\overline{\lambda} = 5(\blacksquare)$

place between the slipping wall and the sphere becomes more complex as a/l and/or λ/a increase(s). Retaining at the most about 50 terms is sufficient to achieve the required eight-digit accuracy for $l/a \geq 1.5$ but much more terms are needed for smaller values of l/a. In addition, more terms are always needed for the modulated shear flow than for the rotating sphere ($N_1^m > N_1^r$ and $N_2^m > N_2^r$). The technique (i) requires more terms than the procedure (ii), except for $\overline{\lambda} > 0$ smaller than unity.

Table 3 Computed torque coefficients c_{zz}^m, c_{zz}^r and dimensionless angular velocity ω (see definition (27)) for different values of the normalized sphere location l/a and wall slip length λ/a. Both (i) and (ii) give identical eight-digit values but need different numbers of terms (N_1^m, N_1^r) and (N_2^m, N_2^r) for convergence

l/a	λ/a	c_{zx}^m	c_{zz}^r	ω	N_1^m	N_1^r	N_2^m	N_2^r
1.001	0	1.08213596	1.19904464	0.90249848	426	384	294	268
1.01	0	1.08047432	1.18324390	0.91314591	129	113	98	89
1.1	0	1.06596885	1.11706475	0.95425879	37	33	33	30
1.5	0	1.03035673	1.03910451	0.99158143	16	14	16	14
2	0	1.01393369	1.01592710	0.99803784	11	10	12	11
5	0	1.00098101	1.00100103	0.99998000	6	6	7	7
10	0	1.00012439	1.00012502	0.99999937	4	4	6	5
1.001	0.5	1.53544181	1.02662233	1.49562481	308	236	296	270
1.01	0.5	1.53046935	1.02639008	1.49111862	97	81	98	90
1.1	0.5	1.48522781	1.02392937	1.45051782	31	28	33	30
1.5	0.5	1.35025068	1.01422153	1.33131731	14	13	16	15
2	0.5	1.25887236	1.00767722	1.24928136	10	9	12	11
5	0.5	1.10081027	1.00074894	1.09998645	5	5	7	7
10	0.5	1.05011282	1.00010793	1.04999949	4	4	6	5
1.001	1	1.99000669	0.98854360	2.01306922	465	339	348	323
1.01	1	1.98180270	0.98919230	2.00345544	146	118	120	112
1.1	1	1.90640944	0.99449092	1.91697017	46	40	41	38
1.5	1	1.67202580	1.00284093	1.66728915	20	19	18	18
2	1	1.50473225	1.00323125	1.49988574	14	13	13	12
5	1	1.20066727	1.00056366	1.19999089	7	6	7	7
10	1	1.10010249	1.00009355	1.09999958	4	4	6	5
1.001	2	2.89693642	0.95734904	3.02599815	722	490	505	450
1.01	2	2.88238911	0.95854471	3.00704711	228	173	178	159
1.1	2	2.74772516	0.96892974	2.83583528	71	60	61	55
1.5	2	2.31631353	0.99138814	2.33643459	30	27	27	25
2	2	1.99710279	0.99829800	2.00050766	20	19	19	17
5	2	1.40042077	1.00030286	1.39999676	9	9	8	8
10	2	1.20008422	1.00007042	1.19999972	6	6	6	5
1.001	5	5.60868606	0.92940232	6.03472356	1320	778	853	684
1.01	5	5.57538703	0.93097804	5.98874176	416	281	306	249
1.1	5	5.26540750	0.94503380	5.57166050	129	99	107	89
1.5	5	4.24860226	0.97919677	4.33886465	54	45	48	41
2	5	3.47485185	0.99248153	3.50117532	36	31	32	28
5	5	1.99978649	0.99989064	2.00000521	14	13	13	12
10	5	1.50003861	1.00002577	1.49999996	8	8	7	7

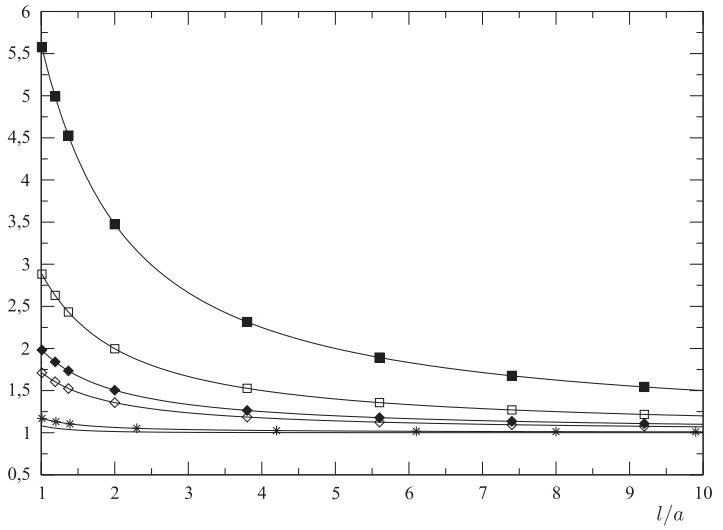

Fig. 3 Torque coefficient c_{zx}^m for $\overline{\lambda} = 0$ (solid line), $\overline{\lambda} = 0.1(*)$, $\overline{\lambda} = 0.7(\Diamond)$, $\overline{\lambda} = 1(\blacklozenge)$, $\overline{\lambda} = 2(\square)$ and $\overline{\lambda} = 5(\blacksquare)$

The coefficient c_{zx}^m is plotted in Fig. 3 versus l/a for several values of $\overline{\lambda}$.

In contrast to c_{zz}^r, it appears that c_{zx}^m might be large for small sphere-wall gap $l/a - 1$ and large $\overline{\lambda}$ and also tends slower to unity for $l/a \gg 1$. Moreover, it turns out that c_{zx}^m increases with $\overline{\lambda}$ for a given sphere location l/a. This is because as the slip length increases the wall ability to let the liquid flow tangent to it is larger. As a consequence, the flow velocity magnitude $|k_m|(z+\lambda)\rho$ on the sphere boundary (in particular on the part facing the wall) strongly increases in a non-trivial way with $\overline{\lambda}$, therefore leading to a larger torque.

For $l + \lambda \gg a$ the ambient fluid velocity is of order $\mathbf{u}_a \sim k_m(l+\lambda)\rho\, \mathbf{e}_\phi$ on the sphere surface. The velocity disturbance $\mathbf{u} = k_m v \mathbf{e}_\varphi$ on the sphere then obeys (14) where the second relation is replaced with the condition $v = \rho(l+\lambda)$. Clearly, the fluid velocity about the sphere is $v = (l+\lambda)v_1$ with $v_1\mathbf{e}_\varphi$ the velocity about a sphere rotating at the angular velocity $\mathbf{e}_3$ near the plane wall with slip length λ. Recalling the definitions (24)–(25) of the coefficients c_{zz}^m and c_{zz}^r, one therefore gets the very first approximations (further improved in section 3.4) $c_{zx}^m \sim (1 + \overline{\lambda}a/l)c_{zz}^r$ and $\omega \sim 1 + \overline{\lambda}a/l$ when $l + \lambda \gg a$. This later condition actually encompasses two different circumstances:

(i) The case of a strongly slipping wall for which $\overline{\lambda} \gg 1$. In this case the sphere location is arbitrary (that is the sphere may even be very close the wall when $l/a \sim 1$).
(ii) The case of a distant sphere with $l/a \gg 1$. Since $a[c_{zz}^r - 1]/l$ vanishes as l/a becomes large (recall Fig. 2) it turns out that $c_{zx}^m \sim 1 + \overline{\lambda}a/l$ for a distant sphere whatever the normalized slip length $\overline{\lambda}$. A refined asymptotic expansion of c_{zx}^m for large l/a will also be derived in section 3.4.

As the reader may check, both approximations $c_{zx}^m \sim (1 + \overline{\lambda}a/l)c_{zz}^r$ and $\omega \sim 1 + \overline{\lambda}a/l$ nicely agree with the computed values presented in Table **3** in the range $l + \lambda \gg a$. For example, taking $l/a = 2$

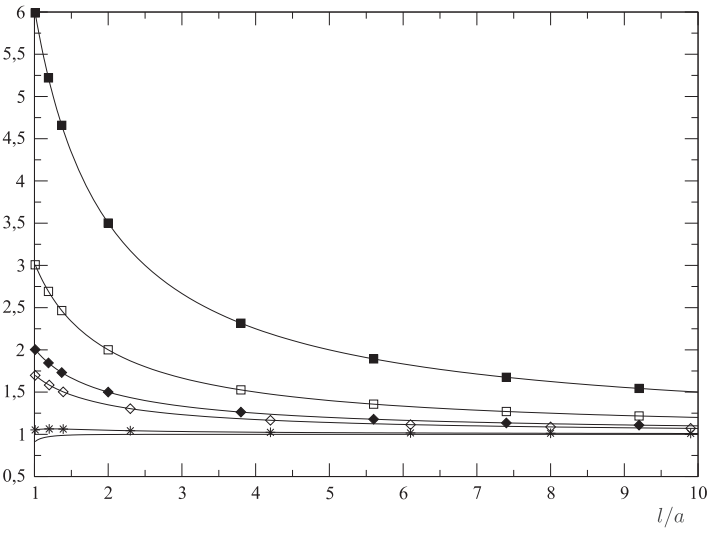

Fig. 4 Normalised angular velocity ω for $\overline{\lambda} = 0$ (solid line), $\overline{\lambda} = 0.1(*)$, $\overline{\lambda} = 0.7(\Diamond)$, $\overline{\lambda} = 1(\blacklozenge)$, $\overline{\lambda} = 2(\square)$ and $\overline{\lambda} = 5(\blacksquare)$

and $\overline{\lambda} = 5$ yields $c_{zx}^m \sim 3.4737$ and $\omega = 3.5$ two values which compare very well with the computed ones ($c_{zx}^m = 3.4748$ and $\omega = 3.501$) reported in Table **3**.

As observed in Fig. 4, the sphere normalized angular velocity ω exhibits the same behaviour as the torque coefficient c_{zx}^m. This is easily understood from (27) since c_{zz}^r generally remains of order unity. Note that for very small $\overline{\lambda}$ the value of ω is less than unity for a sufficiently close sphere. This is because of the local increase of c_{zz}^r due to lubrication stresses.

3.4 *Asymptotic expansions for a distant sphere*

For large l/a asymptotic expansions may be obtained by formally solving (20) using the technique (i) and expanding in terms of the small parameter $\epsilon = \mathrm{e}^{-l/a}$. Results for c_{zx}^m, c_{zz}^r and ω are then obtained as series in a/l each coefficient depending on $\overline{\lambda}$. Like in (**16**), we use for that purpose Maple computer algebra software. The derived asymptotic expansions read

$$c_{zz}^r \sim 1 + \frac{1}{8}(\frac{a}{l})^3 - \frac{3\overline{\lambda}}{8}(\frac{a}{l})^4 + \frac{3\overline{\lambda}^2}{4}(\frac{a}{l})^5, \tag{28}$$

$$c_{zx}^m \sim 1 + \overline{\lambda}(\frac{a}{l}) + \frac{1}{8}(\frac{a}{l})^3 - \overline{\lambda}(\frac{a}{l})^4 + [\frac{3\overline{\lambda}^2}{8} - \frac{1}{16}](\frac{a}{l})^5, \tag{29}$$

$$\omega \sim 1 + \overline{\lambda}(\frac{a}{l}) - \frac{1}{16}(\frac{a}{l})^5. \tag{30}$$

We observe (without formal proof) that (28)–(30) represent asymptotic expansions when $l/a \gg 1$ only for $\overline{\lambda}(a/l) \ll 1$. Instead of plotting (28)–(30) in Figs. 2–4, this later condition is better illustrated

Table 4 Comparisons between computed and asymptotic (given by (28)–(30) and indicated by the $*$ symbols) values of the torque coefficients c_{zz}^m, c_{zz}^r and dimensionless angular velocity ω. The value of $\lambda/l = \overline{\lambda}(a/l)$ is also given

l/a	λ/a	λ/l	c_{zx}^m	$c_{zx}^m(*)$	c_{zz}^r	$c_{zz}^r(*)$	ω	$\omega(*)$
2	0	0	1.01393369	1.01367188	1.01592710	1.01562500	0.99803784	0.99804688
5	0	0	1.00098101	1.00098000	1.00100103	1.00100000	0.99998000	0.99998000
10	0	0	1.00012439	1.00012438	1.00012502	1.00012500	0.99999937	0.99999938
2	0.5	0.25	1.25887236	1.23535156	1.00767722	1.00976563	1.24928136	1.24804688
5	0.5	0.1	1.10081027	1.10021000	1.00074894	1.00076000	1.09998645	1.09998000
10	0.5	0.05	1.05011282	1.05007531	1.00010793	1.00010813	1.04999949	1.04999938
2	1	0.5	1.50473225	1.46289063	1.00323125	1.01562500	1.49988574	1.49804688
5	1	0.2	1.20066727	1.19950000	1.00056366	1.00064000	1.19999089	1.19998000
10	1	0.1	1.10010249	1.10002813	1.00009355	1.00009500	1.09999958	1.09999938
2	2	1	1.99710279	1.93554688	0.99829800	1.06250000	2.00050766	1.99804688
5	2	0.4	1.40042077	1.39826000	1.00030286	1.00076000	1.39999676	1.39998000
10	2	0.2	1.20008422	1.19993938	1.00007042	1.00008000	1.19999972	1.19999938
2	5	2.5	3.47485185	3.49414063	0.99248153	1.48437500	3.50117532	3.49804688
5	5	1	1.99978649	1.99598000	0.99989064	1.00400000	2.00000521	1.99998000
10	5	0.5	1.50003861	1.49971813	1.00002577	1.00012500	1.49999996	1.49999938

by comparing in Table **4** these asymptotic estimates against the computed values for $l/a = 2, 5, 10$ and different values of $\overline{\lambda} = \lambda/a$.

Not surprisingly, the formula (29) yields its worst prediction for $l/a = 2$ and $\overline{\lambda} = 5$. In general, the accuracy of (28)–(30) deteriorates for $l/a = 5, 10$ as $\overline{\lambda}(a/l) = \lambda/l$ increases.

According to (28)–(30) both $c_{zx}^m - 1$ and $\omega - 1$ drop as a/l while $c_{zz}^r - 1$ decays as fast as $(a/l)^3$ for a distant sphere. This property is observed in Figs. 2–4. Finally, it is noteworthy that $\omega - 1 - \overline{\lambda}(a/l) = O((a/l)^5)$ as a/l becomes large.

4. Sphere immersed in quadratic or 'pure' shear flows

This section addresses ambient 'pure' shear and quadratic flows. For symmetry reasons a sphere freely suspended in these flows translates and rotates parallel with $\mathbf{e}_x$ and $\mathbf{e}_y$, respectively. The necessary flow fields $(\mathbf{u}, p)$ are thus solutions of (4)-(5) with the boundary conditions

$$\mathbf{u} = -z^2\mathbf{e}_x \quad \text{on } S \text{ (quadratic shear)}, \qquad \mathbf{u} = -(z+\lambda)\mathbf{e}_x \quad \text{on } S \text{ ('pure' shear)}, \tag{31}$$

$$\mathbf{u} = \mathbf{e}_x \quad \text{on } S \text{ (translation)} \quad , \ \mathbf{u} = \mathbf{e}_y \wedge \mathbf{O'M} \quad \text{on } S \text{ (rotation)}. \tag{32}$$

These flow fields have been obtained in (**10**–**12**) except for the quadratic shear flow which was recently and briefly handled in (**17**, **18**). This section presents for these flow fields a unified treatment reducing, as in (**11**, **12**), to the determination of four series of coefficients (in contrast to (**10**) which ends up with seven series of coefficients). The focus here is on the quadratic shear flow. As

a complement to earlier quoted works, we also calculate the stresslet tensor for the various flow fields.

4.1 *Required flow fields about the sphere*

As pioneered by (**25**, **26**, **27**) for problems with a no-slip solid wall, the velocity and pressure fields $\mathbf{u} = u_\rho \mathbf{e}_\rho + u_\phi \mathbf{e}_\phi + u_z \mathbf{e}_z$ and p are sought for under the following form

$$u_\rho = \frac{1}{2}\{\frac{\rho Q_1}{c} + U_0 + U_2\}\cos\phi,\ u_\phi = \frac{1}{2}(U_2 - U_0)\sin\phi, \tag{33}$$

$$u_z = \frac{1}{2}\{\frac{zQ_1}{c} + 2W_1\}\cos\phi,\ p = \mu Q_1 \cos\phi \tag{34}$$

with $c = a\sinh\alpha$ and unknown functions W_1, U_0, U_1 and U_2 depending upon the bipolar coordinates (η, ξ). The boundary condition $\mathbf{u}.\mathbf{e}_z = 0$ on the $z = \xi = 0$ plane wall and the equation $\mu\nabla^2\mathbf{u} = \nabla p$ in the entire liquid domain $0 < \xi < \alpha$ are enforced by seeking W_1, U_0, U_1, U_2 in the following forms (**14**)

$$W_1 = c^M(\cosh\xi - t)^{1/2}\sin\eta\sum_{n\geq 1} A_n \sinh(\gamma_n\xi)P_n'(t), \tag{35}$$

$$Q_1 = c^M(\cosh\xi - t)^{1/2}\sin\eta\sum_{n\geq 1}[B_n\cosh(\gamma_n\xi) + C_n\sinh(\gamma_n\xi)]P_n'(t), \tag{36}$$

$$U_0 = c^M(\cosh\xi - t)^{1/2}\sum_{n\geq 0}^{\infty}[D_n\cosh(\gamma_n\xi) + E_n\sinh(\gamma_n\xi)]P_n(t), \tag{37}$$

$$U_2 = c^M(\cosh\xi - t)^{1/2}\sin^2\eta\sum_{n\geq 2}[F_n\cosh(\gamma_n\xi) + G_n\sinh(\gamma_n\xi)]P_n''(t), \tag{38}$$

where, recalling (31)–(32), $M = 2$ for the quadratic shear flow, $M = 1$ for the 'pure' shear flow or the sphere rotating parallel with $\mathbf{e}_y$ and $M = 0$ for the sphere translating parallel with $\mathbf{e}_x$. In addition, in (35)–(38) we set $t = \cos\eta$, $\gamma_n = n + 1/2$ while P_n is the Legendre polynomial of order n and primes designate differentiations with respect to t.

Because $(\mathbf{u}, p)$ vanishes as $|\mathbf{OM}| \to \infty$ (that is as $(\xi, \eta) \to (0, 0)$) and is bounded on the wall and in the entire fluid domain, all coefficients A_n, B_n, C_n, D_n, E_n, F_n and G_n are required to vanish as n becomes large.

Exploiting the remaining conditions (5) on the slip wall gives (see **10**, **11**, **12**)

$$cF_n = \frac{c}{2}[A_{n-1} - A_{n+1}] - \frac{\lambda}{4}[C_{n-1} - C_{n+1}]$$
$$-\frac{\lambda}{2}[(n-2)G_{n-1} - (2n+1)G_n + (n+3)G_{n+1}] \quad \text{for } n \geq 2, \tag{39}$$

$$cD_n = \frac{c}{2}[(n+1)(n+2)A_{n+1} - n(n-1)A_{n-1}]$$
$$+\frac{\lambda}{4}[n(n-1)C_{n-1} - (n+1)(n+2)C_{n+1}]$$
$$-\frac{\lambda}{2}[nE_{n-1} - (2n+1)E_n + (n+1)E_{n+1}] \quad \text{for } n \geq 0. \tag{40}$$

As shown in (**26**), the divergence-free condition (4) for the velocity **u** further yields two additional relationships obtained for $\xi > 0$ and $\xi = 0$. The relation for $\xi > 0$ reads

$$(n-2)(n-1)G_{n-1} - 2(n-1)(n+2)G_n + (n+2)(n+3)G_{n+1}$$
$$= (n-1)C_{n-1} - 5C_n - (n+2)C_{n+1} + E_{n-1} - 2E_n + E_{n+1} \quad \text{for } n \geq 1. \tag{41}$$

The second relation for $\xi = 0$ may actually be combined with the boundary conditions for the tangential velocity components on the $\xi = 0$ plane wall thereby providing on this boundary the condition $\partial v_z/\partial z = \lambda \partial^2 v_z/\partial z^2$ for $\xi = 0$. Curtailing the details available in (**12**), we eventually obtain

$$cB_n = c[(n-1)A_{n-1} - (2n+1)A_n + (n+2)A_{n+1}]$$
$$-\lambda[(n-1)C_{n-1} - (2n+1)C_n + (n+2)C_{n+1}] \quad \text{for } n \geq 1, \tag{42}$$

Of course, (39)–(42) hold whatever the addressed flow since (31)–(32) have not yet been taken into account.

Focusing now on the quadratic shear, we further impose (31), that is $\mathbf{u} = -z^2\mathbf{e}_x$ on S. In other words, we require

$$u_\rho = -z^2\cos\phi, \; u_\phi = z^2\sin\phi \qquad \text{and } u_z = 0 \text{ for } \xi = \alpha. \tag{43}$$

Enforcing (43), as detailed in Appendix A, results in three additional relationships. Defining

$$q_n^- = \frac{\tanh(\gamma_n\alpha)}{\tanh\alpha} - 1, \; q_n^+ = \frac{\tanh(\gamma_n\alpha)}{\tanh\alpha} + 1, \; \gamma_n = n + \frac{1}{2} \quad \text{for } n \geq 0, \tag{44}$$

these relations read

$$B_n = 2q_n^-\left(\frac{n-1}{2n-1}\right)A_{n-1} + 2q_n^+\left(\frac{n+2}{2n+3}\right)A_{n+1}$$
$$-\tanh(\gamma_n\alpha)[C_n + 2A_n/\tanh\alpha] + f_n^{(M)} \quad \text{for } n \geq 1, \tag{45}$$

$$D_n = \frac{(n+1)(n+2)}{2n+3}q_n^+A_{n+1} - \frac{n(n-1)}{2n-1}q_n^-A_{n-1}$$
$$-\tanh(\gamma_n\alpha)E_n - K_n^{(M)} \quad \text{for } n \geq 0, \tag{46}$$

$$F_n = \frac{q_n^-}{2n-1}A_{n-1} - \frac{q_n^+}{2n+3}A_{n+1} - \tanh(\gamma_n\alpha)G_n + f_n^{(M)} \quad \text{for } n \geq 2, \tag{47}$$

with, for the quadratic shear flow ($M = 2$),

$$K_n^{(2)} = \frac{8\sqrt{2}\gamma_n \mathrm{e}^{-\gamma_n\alpha}}{3\cosh(\gamma_n\alpha)}[\gamma_n + \coth\alpha] \qquad \text{for } n \geq 0 \text{ and } f_n^{(2)} = 0 \text{ for } n \geq 1. \tag{48}$$

As established in (**10**–**12**), (45)–(47) still hold for the other boundary conditions (31)–(32):

(i) For the sphere held fixed in the pure shear flow $(\lambda + z)\mathbf{e}_x$, then $M = 1$ and

$$K_n^{(1)} = \frac{4\sqrt{2}\mathrm{e}^{-\gamma_n\alpha}}{\cosh(\gamma_n\alpha)}[\gamma_n + \frac{\lambda}{2c}] \qquad \text{for } n \geq 0 \text{ and } f_n^{(1)} = 0 \text{ for } n \geq 1. \tag{49}$$

(ii) For the sphere translating with velocity $\mathbf{e}_x$, then $M = 0$ and

$$K_n^{(0)} = -\frac{2\sqrt{2}\mathrm{e}^{-\gamma_n\alpha}}{\cosh(\gamma_n\alpha)} \qquad \text{for } n \geq 0 \text{ and } f_n^{(0)} = 0 \text{ for } n \geq 1. \tag{50}$$

(iii) For the sphere rotating with velocity $\mathbf{e}_y$, then $M = 1$ and

$$K_n^{(1)} = \gamma_n[\frac{q_n^-}{\sinh(\gamma_{n-1}\alpha)} - \frac{2\sqrt{2}\mathrm{e}^{-\gamma_n\alpha}}{\cosh(\gamma_n\alpha)}] \qquad \text{for } n \geq 0, \tag{51}$$

$$f_n^{(1)} = \frac{4\gamma_n q_n^-}{\sinh(\gamma_{n-1}\alpha)} \qquad \text{for } n \geq 1. \tag{52}$$

As proposed in (**11**, **12**) and in contrast to (**10**), the task of determining the coefficients A_n, C_n, E_n and G_n may be reduced as follows. Injecting (45)–(47) in (39)–(41) and setting $\overline{\lambda} = \lambda/a$ provides the following coupled equations

$$\begin{aligned}
&(\frac{n-1}{2n-1})(2n-1-2q_n^-)A_{n-1} + 2[\coth\alpha\tanh(\gamma_n\alpha) - \gamma_n]A_n \\
&\quad +(\frac{n+2}{2n+3})(2n+3-2q_n^+)A_{n+1} - \frac{(n-1)\overline{\lambda}}{\sinh\alpha}C_{n-1} \\
&\quad +[\frac{(2n+1)\overline{\lambda}}{\sinh\alpha} + \tanh(\gamma_n\alpha)]C_n - \frac{(n+2)\overline{\lambda}}{\sinh\alpha}C_{n+1} = 0 \quad \text{for } n \geq 1,
\end{aligned} \tag{53}$$

$$\begin{aligned}
&-[\frac{2q_n^- - 2n + 1}{2(2n-1)}]A_{n-1} - [\frac{2n+3-2q_n^+}{2(2n+3)}]A_{n+1} \\
&\quad -\frac{\overline{\lambda}}{4\sinh\alpha}[C_{n-1} - C_{n+1}] - \frac{\overline{\lambda}}{2\sinh\alpha}[(n-2)G_{n-1} + (n+3)G_{n+1}] \\
&\quad +[\frac{\overline{\lambda}}{\sinh\alpha}\gamma_n + \tanh(\gamma_n\alpha)]G_n = f_n^{(M)} \quad \text{for } n \geq 2,
\end{aligned} \tag{54}$$

$$-[\frac{n(n-1)}{2(2n-1)}][2q_n^- + 2n - 1]A_{n-1} + [\frac{(n+1)(n+2)}{2(2n+3)}][2q_n^+ - 2n - 3]A_{n+1}$$
$$-\frac{n(n-1)\overline{\lambda}}{4\sinh\alpha}C_{n-1} + \frac{(n+1)(n+2)\overline{\lambda}}{4\sinh\alpha}C_{n+1} + \frac{n\overline{\lambda}}{2\sinh\alpha}E_{n-1}$$
$$-[\frac{\overline{\lambda}}{\sinh\alpha}\gamma_n + \tanh(\gamma_n\alpha)]E_n + \frac{(n+1)\overline{\lambda}}{2\sinh\alpha}E_{n+1} = K_n^{(M)} \quad \text{for } n \geq 0, \tag{55}$$

$$(n-2)(n-1)G_{n-1} - 2(n-1)(n+2)G_n + (n+2)(n+3)G_{n+1}$$
$$= (n-1)C_{n-1} - 5C_n - (n+2)C_{n+1} + E_{n-1} - 2E_n + E_{n+1} \quad \text{for } n \geq 1. \tag{56}$$

Because **u** vanishes far from the sphere it is also (see (**10**)) required that

$$(A_n, C_n, E_n, G_n) \to (0, 0, 0, 0) \quad \text{as } n \to \infty. \tag{57}$$

In this process, once A_n, C_n, E_n and G_n are obtained, the coefficients B_n, D_n and F_n follow from (45) to (47).

4.2 *Resulting force, torque and stresslet tensor*

This section expresses the force, torque and second-rank stresslet tensor exerted on the sphere by each of the previously-handled flow fields of the form (33)–(38).

4.2.1 General formulae. From (**25**, **26**), the net force and torque (about the sphere centre O') produced on the sphere by a flow field given by (33)–(38) read

$$\mathbf{F} = \int_S \boldsymbol{\sigma}.\mathbf{n}dS = F_x\mathbf{e}_x, \;\; F_x = -\sqrt{2}\pi\mu c^{M+1}F(C_n; E_n), \tag{58}$$

$$\mathbf{T} = \int_S \mathbf{O'M} \wedge \boldsymbol{\sigma}.\mathbf{n}dS = T_y\mathbf{e}_y, \;\; T_y = 2\sqrt{2}\pi\mu c^{M+2}T(A_n; E_n)\mathbf{e}_y, \tag{59}$$

with F and T expressed in terms of the coefficients A_n, C_n and E_n as follows

$$F(C_n; E_n) = \sum_{n\geq 0}[n(n+1)C_n + E_n], \;\; T(A_n; E_n) = \sum_{n\geq 0}[2n(n+1)A_n + \frac{E_n}{\tanh\alpha}]. \tag{60}$$

Another quantity of interest is the second-rank stresslet tensor **S** exerted on the sphere. When defined with respect to the sphere centre O' it reads

$$\mathbf{S} = \frac{1}{2}\int_S \left\{\mathbf{x}' \otimes \boldsymbol{\sigma}.\mathbf{n} + \boldsymbol{\sigma}.\mathbf{n} \otimes \mathbf{x}' - \frac{2}{3}(\mathbf{x}'.\boldsymbol{\sigma}.\mathbf{n})\mathbf{I}\right\}dS \tag{61}$$

with $\mathbf{x}' = \mathbf{O'M}$ and **I** the usual identity tensor. The stresslet **S** plays a key role (see, among others, (**28**–**31**)) in the theoretical prediction of the effective viscosity of a *dilute* suspension of

freely-suspended solid spheres. It is thus expected to be useful for a dilute suspension bounded by a slipping plane wall and subject to a prescribed ambient linear or quadratic shear flow given by (9).

For a disturbed flow field of the general form (33)–(34) symmetries easily show that $\mathbf{S} = S_{xz}[\mathbf{e}_x \otimes \mathbf{e}_z + \mathbf{e}_z \otimes \mathbf{e}_x]$. Moreover, (61) yields $S_{xz} = D_{xz} + \mathbf{T}.\mathbf{e}_y/2$ with D_{xz} the following Cartesian component of a Stokes doublet

$$D_{xz} = \int_S (\mathbf{x}'.\mathbf{e}_x)(\mathbf{e}_z.\boldsymbol{\sigma}.\mathbf{n})dS. \tag{62}$$

As shown in (**32**), the component D_{xz} may be expressed in terms of the coefficients A_n, B_n and C_n by exploiting (33)–(38). Taking into account (58)–(59), we eventually obtain

$$S_{xz} = \sqrt{2}\pi\mu c^{M+2} S(B_n; C_n; E_n), \tag{63}$$

$$S(B_n; C_n; E_n) = -\sum_{n\geq 0}[\frac{n(n+1)(2n+1)}{3}(B_n + C_n) - \frac{E_n}{\tanh\alpha}]. \tag{64}$$

4.2.2 Resulting force, torque and stresslet friction coefficients. From (58) to (59) and (63) we introduce force, torque and stresslet (normalised) friction factors associated with the non-zero components F_x, T_y and S_{xz} for a sphere held fixed in a pure or quadratic shear flow and a sphere either translating or rotating parallel with $\mathbf{e}_x$ or $\mathbf{e}_y$, respectively. The adopted definitions are displayed below.

(1) Sphere held fixed in the pure shear flow $k_s(\lambda + z)\mathbf{e}_x$. We designate by $(A_n^s; B_n^s; C_n^s; E_n^s)$ the coefficients obtained for $k_s = 1$, and introduce the friction factors f_{xx}^s, c_{yx}^s and s_{xz}^s as*

$$F_x^s = 6\pi\mu a(l+\lambda)k_s f_{xx}^s,\ T_y^s = 4\pi\mu a^3 k_s c_{yx}^s,\ S_{xz} = \frac{10}{3}\pi\mu a^3 k_s s_{xz}^s. \tag{65}$$

(2) Sphere translating with the velocity $U\mathbf{e}_x$. In this case $(A_n^t; B_n^t; C_n^t; E_n^t)$ are the coefficients derived for $U = 1$ and the friction factors f_{xx}^t, c_{yx}^t and s_{xz}^t are defined from

$$F_x^t = -6\pi\mu a U f_{xx}^t,\ T_y^t = 8\pi\mu a^2 U c_{yx}^t,\ S_{xz}^t = 6\pi\mu a^2 U s_{xz}^t. \tag{66}$$

(3) Sphere rotating with the velocity $\Omega\mathbf{e}_y$. The coefficients for $\Omega = 1$ are denoted by $(A_n^r; B_n^r; C_n^r; E_n^r)$ and the friction factors f_{xy}^r, c_{yy}^r and s_{xz}^r are such that

$$F_x^r = 6\pi\mu a^2\Omega f_{xy}^r,\ T_y^r = -8\pi\mu a^3\Omega c_{yy}^r,\ S_{xz}^r = 6\pi\mu a^3\Omega s_{xz}^r. \tag{67}$$

(4) Sphere held fixed in the quadratic shear flow $k_q z^2\mathbf{e}_x$. We label $(A_n^q; B_n^q; C_n^q; E_n^q)$ the coefficients obtained for $k_q = 1$ and use the friction factors f_{xx}^q, c_{yx}^q and s_{xz}^q satisfying

$$F_x^q = 6\pi\mu a l^2 k_q f_{xx}^q,\ T_y^q = 8\pi\mu a^3 l k_q c_{yx}^q,\ S_{xz}^r = \frac{20}{3}\pi\mu a^3 l k_q s_{xz}^q. \tag{68}$$

* A misprint error in (**11**) in the definition of f_{xx}^s was corrected in (**12**).

Setting $z = z' + l$, the following decompositions hold

$$k_s(z+\lambda) = k_s z' + k_s(l+\lambda), \quad k_q z^2 = 2k_q l z' + k_q(l^2 + z'^2). \tag{69}$$

Accordingly, for a distant sphere (a case for which the results for an unbounded liquid prevail) the non-zero contribution to S_{xz} is due to the velocity $k_s z' \mathbf{e}_z$ or $2k_q l z' \mathbf{e}_z$ for the ambient pure shear or quadratic shear flow, respectively. This explains the selected scalings for S_{xz} in (65) and (68).

It is noteworthy that the usual reciprocal identity (**19**) also holds (see, for instance, (**12**)) for two arbitrary Stokes flows satisfying (4)–(6) with $\mathbf{u}_a = \mathbf{0}$. Consequently, $f^r_{xy} = 4c^t_{yx}/3$. All coefficients $f^t_{xx}, c^t_{yx}, f^r_{xy}, f^s_{xx}, c^s_{yx}, s^t_{xz}, s^r_{xz}$ and s^s_{xz}, also termed friction factors, are then displayed in Appendix B whereas for the quadratic shear flow the results are

$$f^q_{xx} = -\frac{\sqrt{2}}{6}\frac{\sinh^3\alpha}{\cosh^2\alpha}F(C^q_n; E^q_n),\ c^q_{yx} = \frac{\sqrt{2}}{4}\frac{\sinh^4\alpha}{\cosh\alpha}T(A^q_n; E^q_n), \tag{70}$$

$$s^q_{xz} = \frac{3\sqrt{2}}{20}\frac{\sinh^4\alpha}{\cosh\alpha}S(B^q_n; C^q_n; E^q_n). \tag{71}$$

Each friction factor depends upon $(\lambda/a, l/a)$. The values in absence of wall, further denoted by using the additional superscript *NW* (which means no wall), are obtained by using the widely-employed Faxen relations (see **24**, **19**) for a *solid sphere* and found to be unity except the following ones

$$f^{q,NW}_{xx} = 1 + \frac{1}{3}(\frac{a}{l})^2,\ f^{r,NW}_{xy} = c^{t,NW}_{yx} = s^{t,NW}_{xz} = s^{r,NW}_{xz} = 0. \tag{72}$$

Accordingly, $f^r_{xy}, c^t_{yx}, s^t_{xz}$ and s^r_{xz} vanish while the other friction factors tend to unity as l/a becomes large.

4.3 *Case of a freely-suspended sphere*

A *freely-suspended* sphere in the quadratic ambient shear flow field $k_q z^2 \mathbf{e}_x$ translates with velocity $U_q \mathbf{e}_x$ and rotates at the angular velocity $\Omega_q \mathbf{e}_y$. These velocities are derived by enforcing the relations (8). Exploiting the definitions (66)–(68) provides the following normalized velocities u_q and ω_q

$$u_q = \frac{U_q}{k_q(l^2 + \frac{a^2}{3})} = \frac{(\frac{l}{a})^2 c^r_{yy} f^q_{xx} + (\frac{l}{a}) f^r_{xy} c^q_{yx}}{[(\frac{l}{a})^2 + \frac{1}{3}][c^r_{yy} f^t_{xx} - f^r_{xy} c^t_{yx}]}, \tag{73}$$

$$\omega_q = \frac{\Omega_q}{k_q l} = \frac{c^q_{yx} f^t_{xx} + (\frac{l}{a}) f^q_{xx} c^t_{yx}}{c^r_{yy} f^t_{xx} - f^r_{xy} c^t_{yx}}. \tag{74}$$

By superposition, the stress tensor component $S^{q,\text{free}}_{xz}$ for a sphere freely suspended in the quadratic shear flow and its associated dimensionless component $s^{q,\text{free}}_{xz}$ are given by

$$s^{q,\text{free}}_{xz} = \frac{S^{q,\text{free}}_{xz}}{\frac{20}{3}\pi\mu a^3 l k_q} = \big(\frac{9}{10}\frac{l}{a} + \frac{3}{10}\frac{a}{l}\big)s^t_{xz}u_q + \frac{9}{10}s^r_{xz}\omega_q + s^q_{xz}. \tag{75}$$

Similarly, a sphere *freely-suspended* in the pure shear flow field $k_s(z+\lambda)\mathbf{e}_x$ translates with velocity $U_s\mathbf{e}_x$ and rotates with velocity $\Omega_s\mathbf{e}_y$ given by**

$$u_s = \frac{U_s}{k_s(l+\lambda)} = \frac{c^r_{yy}f^s_{xx} + (\frac{l}{a}+\frac{\lambda}{a})^{-1}f^r_{xy}c^s_{yx}/2}{[c^r_{yy}f^t_{xx} - f^r_{xy}c^t_{yx}]}, \tag{76}$$

$$\omega_s = \frac{\Omega_s}{k_s/2} = \frac{c^s_{yx}f^t_{xx} + 2(\frac{l}{a}+\frac{\lambda}{a})f^s_{xx}c^t_{yx}}{c^r_{yy}f^t_{xx} - f^r_{xy}c^t_{yx}} \tag{77}$$

whereas the associated stress tensor component $S^{s,\text{free}}_{xz}$ and selected normalised component $s^{s,\text{free}}_{xz}$ read

$$s^{s,\text{free}}_{xz} = \frac{S^{q,\text{free}}_{xz}}{\frac{10}{3}\pi\mu a^3 k_s} = \frac{9}{5}(\frac{l}{a}+\frac{\lambda}{a})s^t_{xz}u_s + \frac{9}{10}s^r_{xz}\omega_s + s^s_{xz}. \tag{78}$$

Note that each quantity u_q, ω_q, $s^{q,\text{free}}_{xz}$, u_s, ω_s and $s^{s,\text{free}}_{xz}$ tends to unity as a/l vanishes.

5. Asymptotic and numerical results for the linear and quadratic shear flows

This section briefly presents the numerical treatment. It then gives asymptotic results for a distant sphere and numerical results for a sphere with arbitrary location.

5.1 *Computational methods*

We first cast the equations (53)–(56) into the following form

$$\hat{M}_1X_1 + \hat{M}^+_1X_2 = B_1, \tag{79}$$

$$M^-_nX_{n-1} + M_nX_n + M^+_nX_{n+1} = B_n \qquad (n \geq 2), \tag{80}$$

where the M's are 4×4 known matrices are readily obtained by inspecting (53)–(56) and the vectors X_n are defined as

$$X_1 = \vec{A}_1C_1E_1E_0,\ X_n = \vec{A}_nC_nE_nG_n \quad (n \geq 2) \tag{81}$$

while the right-hand sides vectors B_n read

$$B_1 = \vec{0}K^{(M)}_0K^{(M)}_1 0,\ B_n = \vec{0}f^{(M)}_nK^{(M)}_n 0 \quad (n \geq 2). \tag{82}$$

Of course, the infinite linear system (79)–(82) is supplemented with the key asymptotic behaviour (57). It is inverted by truncating at a large enough integer N when setting $X_{N+1} = (0, 0, 0, 0)^t$. For a prescribed level of truncation N two different approaches have been employed to solve the resulting truncated linear system with $4N \times 4N$ matrix M_s:

(i) A direct solution by applying a LU factorization algorithm to the matrix M_s (see section 5.2).
(ii) The use of a so-called Thomas' algorithm to efficiently handle the obtained sparse and tridiagonal matrix M_s. Details regarding the relevant implementation are given in (**17**) (see section 5.3).

** Errors made for both u_s and ω_s in (**17**) were corrected in (**12**).

Table 5 Computed normalised friction factors and velocities versus the truncating integer N when inverting the linear system (79)–(80) by Gaussian elimination (direct approach (i) in section 5.1). Here the wall slip length is large and the wall-sphere gap is small with $\lambda/a = 5$ and $l/a = 1.005$

	$N = 4000$	$N = 8000$	$N = 12000$	$N = 16000$
f^t_{xx}	0.98621160	0.98621211	0.98621211	0.98621211
c^t_{yx}	−0.13224102	−0.13244200	−0.13244240	−0.13244240
c^r_{yy}	1.44741109	1.44746265	1.44746265	1.44746275
f^s_{xx}	0.98621160	0.98621211	0.98621211	0.98621211
c^s_{yx}	2.25502664	2.25753149	2.25753648	2.25753651
f^q_{xx}	1.41806687	1.41806778	1.41806778	1.41806778
c^q_{yx}	0.95468458	0.95504181	0.95504252	0.95504253
u_s	1.00440183	1.00440125	1.00440125	1.00440125
ω_s	0.45586282	0.45590285	0.45590293	0.45590293
u_q	1.00925708	1.00925169	1.00925168	1.00925168
ω_q	0.53632655	0.53636760	0.53636768	0.53636768
s^t_{xz}	0.02184178	0.02197565	0.02197592	0.02197592
s^r_{xz}	0.52201099	0.52037626	0.52037299	0.52037298
s^s_{xz}	0.82941082	0.84547752	0.84550956	0.84550978
s^q_{xz}	1.01431902	1.01661042	1.01661500	1.01661502
$s^{s,free}_{xz}$	1.28070678	1.29757473	1.29760836	1.29760860
$s^{q,free}_{xz}$	1.29280961	1.29449355	1.29449690	1.29449693

5.2 *Numerical technique*

The truncation level N is iteratively increased until a prescribed accuracy is reached for the computed vectors X_n. As for the modulated rotational flow (see section 3.3), the value of N required to reach a prescribed accuracy in the determination of a normalised quantity (friction factor or normalised velocity) depends on the addressed quantity and increases as the wall slip length increases and/or the sphere approaches the slipping wall. This trend is illustrated in Table **5**, using the previous direct LU factorization algorithm (i), for $\lambda/a = 5$ and $l/a = 1.005$ (a severe setting requiring N to be large since the wall-sphere gap is small compared with both the sphere radius and the wall slip length). Note that results for translation, rotation and linear shear flow are in perfect agreement with those of (**12**) which used method (ii) (except for the stresslet which was not treated there).

As confirmed by this Table **5**, taking $N = 12000$ is 'sufficient' to compute all the normalised quantity introduced in section 4.2 and section 4.3 with a six-digit accuracy in the range $0 \leq \lambda/a \leq 5$ when $l/a \geq 1.005$. Note that, in this regard, the more demanding quantities are the stresslet friction factors. Still smaller gaps would need a larger number of terms. Method (ii) would also need a larger

number of digits, since it is explicit (see (**12**) for details in the cases of translation, rotation and pure shear flow).

5.3 *Asymptotic analysis for a distant sphere*

For engineering applications it is useful to propose handy formulae for the friction coefficients which are valid in a wide range of values of the slip length and sphere location. It is worth quantifying the range of the sphere-wall interactions by scaling them in terms of the small parameter $a/l \ll 1$ and λ/a for a distant sphere. We define in this article 'long-range' as being $O(a/l)$ and 'short-range' as decaying faster than $O(a/l)$. The asymptotic estimate of a given friction coefficient or normalized velocity is expected to depend upon the addressed quantity for a fixed or a freely-suspended distant sphere, that is for $a/l \ll 1$. It is here obtained by Thomas' algorithm, with Mathematica computer algebra software, expanding the friction coefficient in terms of the small parameter $\epsilon = \mathrm{e}^{-l/a}$ and then converting the result as series in a/l. In doing so we retain in the series (35)–(38) one more term than the desired number of terms in ϵ for the velocities W_1, U_0, U_2 and pressure Q_1. The method is by essence able to build asymptotic expansions at large orders. For a sake of conciseness, attention is however restricted in this article to estimates of order $(a/l)^5$.

5.3.1 Sphere translating or rotating parallel to a distant slipping wall. Friction coefficients $c^r_{yy}, f^r_{xy} = 4c^t_{yx}/3$ and f^t_{xx} have been numerically computed for arbitrary sphere location and normalised slip length $\overline{\lambda} = \lambda/a$ in (**10**) and more recently, at a high-level accuracy, also in (**12**). However, those papers neither provide asymptotic estimates nor consider the stresslet factors s^t_{xz} and s^r_{xz}. Here, we obtain for a distant rotating sphere

$$c^r_{yy} \sim 1 + \frac{5}{16}\left(\frac{a}{l}\right)^3 - \frac{15\overline{\lambda}}{16}\left(\frac{a}{l}\right)^4 + \frac{27\overline{\lambda}^2}{8}\left(\frac{a}{l}\right)^5, \tag{83}$$

$$f^r_{xy} \sim [\frac{1}{8} - \frac{9\overline{\lambda}^2}{8}]\left(\frac{a}{l}\right)^4 - [\frac{3}{64} + \frac{\overline{\lambda}}{2} + \frac{81\overline{\lambda}^2}{128} - \frac{33\overline{\lambda}^3}{4}]\left(\frac{a}{l}\right)^5, \tag{84}$$

$$s^r_{xz} \sim \frac{5}{24}\left(\frac{a}{l}\right)^3 - \frac{5\overline{\lambda}}{8}\left(\frac{a}{l}\right)^4 - [\frac{1}{6} - \frac{55\overline{\lambda}^2}{12}]\left(\frac{a}{l}\right)^5 \tag{85}$$

and for a distant translating sphere

$$\begin{aligned} f^t_{xx} \sim 1 &+ \frac{9}{16}\left(\frac{a}{l}\right) + [\frac{81}{256} - \frac{9\overline{\lambda}}{16}]\left(\frac{a}{l}\right)^2 + [\frac{217}{4096} - \frac{81\overline{\lambda}}{128} + \frac{9\overline{\lambda}^2}{8}]\left(\frac{a}{l}\right)^3 \\ &+ [\frac{8865}{65536} - \frac{651\overline{\lambda}}{4096} + \frac{405\overline{\lambda}^2}{256} - \frac{81\overline{\lambda}^3}{16}]\left(\frac{a}{l}\right)^4 \\ &+ [\frac{207529}{1048576} - \frac{8865\overline{\lambda}}{16384} - \frac{2655\overline{\lambda}^2}{4096} - \frac{891\overline{\lambda}^3}{128} + \frac{261\overline{\lambda}^4}{8}]\left(\frac{a}{l}\right)^5, \end{aligned} \tag{86}$$

$$\begin{aligned} s^t_{xz} \sim &\frac{5}{16}\left(\frac{a}{l}\right)^2 + [\frac{45}{256} - \frac{5\overline{\lambda}}{8}]\left(\frac{a}{l}\right)^3 - [\frac{619}{4096} + \frac{135\overline{\lambda}}{256} - \frac{45\overline{\lambda}^2}{16}]\left(\frac{a}{l}\right)^4 \\ &+ [\frac{11069}{65536} + \frac{619\overline{\lambda}}{1024} + \frac{585\overline{\lambda}^2}{256} - \frac{145\overline{\lambda}^3}{8}]\left(\frac{a}{l}\right)^5. \end{aligned} \tag{87}$$

Table 6 Comparisons between computed and asymptotic values (see (88)–(99)) of the normalized friction factors and velocities for $\lambda = a$ and $l/a = 10, 100$

	Computed $l = 10a$	Asymptotic $l = 10a$	Computed $l = 100a$	Asymptotic $l = 100a$
f^t_{xx}	1.05412	1.05423	1.0056009030	1.0056009032
f^r_{xy}	−0.00058	−0.00029	−0.0000000094	−0.0000000093
c^r_{yy}	1.00024	1.00025	1.0000003034	1.0000003035
f^s_{xx}	1.05387	1.05397	1.0056005979	1.0056005981
c^s_{yx}	1.00095	1.00121	1.0000014147	1.0000014151
f^q_{xx}	1.05708	1.05718	1.0056338068	1.0056338069
c^q_{yx}	1.00042	1.00057	1.0000007002	1.0000007005
u_s	0.99976	0.99975	0.9999996965	0.9999996965
ω_s	0.99974	0.99972	0.9999996963	0.9999996962
u_q	0.99947	0.99945	0.9999993872	0.9999993870
ω_q	0.99974	0.99975	0.9999996963	0.9999996966
s^t_{xz}	0.00280	0.00274	0.0000308207	0.0000308206
s^r_{xz}	0.00017	0.00019	0.0000002025	0.0000002025
s^s_{xz}	0.94511	0.94431	0.9943975227	0.9943975224
s^q_{xz}	0.97530	0.97486	0.9972267727	0.9972267719
$s^{s,free}_{xz}$	1.00075	1.00083	1.0000009109	1.0000009111
$s^{q,free}_{xz}$	1.00075	1.00080	1.0000009109	1.0000009109

For a no-slip wall ($\bar{\lambda} = 0$) the terms of order $(a/l)^4$ vanish in the expansions of c^r_{yy} and s^r_{xz} and the results match the ones derived earlier in (**16**) for the force and torque friction factors. A non-zero normalised wall slip length $\bar{\lambda}$ affects some coefficients of the previous expansions but, except for f^r_{xy}, not the leading term. As a result, the above friction factors are more or less sensitive to the wall slip length when the sphere is distant. For instance, c^r_{yy} is weakly sensitive to the wall slip while f^r_{xy} (and also c^t_{yx}) is even less affected. Finally, observe that some terms in the expansions (86)–(87) adopt a complicated form.

The proposed asymptotic expansions are compared in Table **6** for $\bar{\lambda} = 1$ and $l/a = 10, 100$ with the computed values obtained by using the LU factorisation algorithm with $N = 12000$ (this value of N has been found to give the reported 10-digit accuracy for these values of $(\bar{\lambda}, l/a)$).

5.3.2 Sphere in a shear flow bounded by a distant slipping wall. We now turn to the asymptotic results for a sphere immersed in a linear or quadratic ambient shear flow. For the linear shear flow neither (**10**) nor (**12**) provided such asymptotic estimates. For a distant sphere *held fixed* in the pure

shear flow $k_s(z+\lambda)\mathbf{e}_x$ we obtain

$$f^s_{xx} \sim 1 + \frac{9}{16}\left(\frac{a}{l}\right) - \left(\frac{9\overline{\lambda}}{16} - \frac{81}{256}\right)\left(\frac{a}{l}\right)^2 - \left(\frac{1063}{4096} + \frac{81\overline{\lambda}}{128} - \frac{9\overline{\lambda}^2}{8}\right)\left(\frac{a}{l}\right)^3$$
$$-[\frac{2655}{65536} - \frac{3189\overline{\lambda}}{4096} - \frac{405\overline{\lambda}^2}{256} + \frac{81\overline{\lambda}^3}{16}]\left(\frac{a}{l}\right)^4$$
$$+[\frac{300457}{1048576} + \frac{2655\overline{\lambda}}{16384} - \frac{15711\overline{\lambda}^2}{4096} - \frac{1782\overline{\lambda}^3}{256} + \frac{261\overline{\lambda}^4}{8}]\left(\frac{a}{l}\right)^5, \tag{88}$$

$$c^s_{yx} \sim 1 - \frac{3}{16}(1 - 9\overline{\lambda}^2)\left(\frac{a}{l}\right)^3 + \frac{9}{256}(2 + 16\overline{\lambda} + 27\overline{\lambda}^2 - 304\overline{\lambda}^3)\left(\frac{a}{l}\right)^4$$
$$+(\frac{593}{2048} - \frac{9\overline{\lambda}}{32} - \frac{24437\overline{\lambda}^2}{4096} - \frac{891\overline{\lambda}^3}{128} + \frac{1197\overline{\lambda}^4}{16})\left(\frac{a}{l}\right)^5, \tag{89}$$

$$s^s_{xz} \sim 1 - \frac{9}{16}\left(\frac{a}{l}\right) + \left(\frac{9\overline{\lambda}}{16} - \frac{81}{256}\right)\left(\frac{a}{l}\right)^2 + \left(\frac{20931}{20480} + \frac{81\overline{\lambda}}{128} - \frac{63\overline{\lambda}^2}{16}\right)\left(\frac{a}{l}\right)^3$$
$$-\left(\frac{42021}{327680} + \frac{62793\overline{\lambda}}{20480} + \frac{405\overline{\lambda}^2}{128} - \frac{441\overline{\lambda}^3}{16}\right)\left(\frac{a}{l}\right)^4$$
$$-\left(\frac{6128717}{5242880} - \frac{42021\overline{\lambda}}{81920} - \frac{222293\overline{\lambda}^2}{10240} - \frac{5427\overline{\lambda}^3}{256} + \frac{3483\overline{\lambda}^4}{16}\right)\left(\frac{a}{l}\right)^5. \tag{90}$$

Again, for $\overline{\lambda} = 0$ above results (88)-(89) match those of (**16**). Thus, one has either long-range (for f^s_{xx} and s^s_{xz}) or short-range (case of c^s_{yx}) sphere–wall interactions for a sphere *held fixed* in the linear shear flow. Moreover, exploiting (76)–(78), (83)–(84), (86) and (88)–(89) gives for a *freely-suspended* sphere in a pure shear flow the approximations

$$u_s \sim 1 - \frac{5}{16}\left(\frac{a}{l}\right)^3 + \frac{15\overline{\lambda}}{16}\left(\frac{a}{l}\right)^4 + \left(\frac{1}{4} - \frac{15\overline{\lambda}^2}{4}\right)\left(\frac{a}{l}\right)^5, \tag{91}$$

$$\omega_s \sim 1 - \frac{5}{16}\left(\frac{a}{l}\right)^3 + \frac{15\overline{\lambda}}{16}\left(\frac{a}{l}\right)^4 + \left(\frac{1}{4} - \frac{55\overline{\lambda}^2}{8}\right)\left(\frac{a}{l}\right)^5, \tag{92}$$

$$s^{s,\text{free}}_{xz} \sim 1 + \frac{15}{16}\left(\frac{a}{l}\right)^3 - \frac{45\overline{\lambda}}{16}\left(\frac{a}{l}\right)^4 - \left(1 - \frac{145\overline{\lambda}^2}{8}\right)\left(\frac{a}{l}\right)^5. \tag{93}$$

As seen again in Table **6**, the proposed estimates (88)–(93) agree with the computed values. Moreover, the formulae (91)–(93) reveal that the rigid-body motion and the stresslet experienced by a distant sphere ($\epsilon = a/l \ll 1$) freely suspended in a pure linear shear flow are solely affected at order $O(\epsilon^3)$

by the wall regardless of slip and at order $O(\epsilon^4)$ by the wall normalized slip length $\overline{\lambda}$. Finally, note also that $u_s - \omega_s = O(\epsilon^5)$ whatever $\overline{\lambda} > 0$ when $l \gg a$.

In a similar way, asymptotic estimates of the factors f^q_{xx}, c^q_{yx} and s^q_{xz} for a distant sphere held fixed in a quadratic shear flow have been given, up to order $(a/l)^6$, in (**17**). Retaining here expansions up to order $(a/l)^5$,

$$f^q_{xx} \sim 1 + \frac{9}{16}\left(\frac{a}{l}\right) + \left(\frac{499}{768} - \frac{9\overline{\lambda}}{16}\right)\left(\frac{a}{l}\right)^2 + \left(\frac{9\overline{\lambda}^2}{8} - \frac{81\overline{\lambda}}{128} - \frac{1575}{4096}\right)\left(\frac{a}{l}\right)^3 - \left(\frac{81\overline{\lambda}^3}{16} - \frac{405\overline{\lambda}^2}{256} - \frac{3701\overline{\lambda}}{4096} + \frac{7263}{65536}\right)\left(\frac{a}{l}\right)^4 + \left(\frac{261\overline{\lambda}^4}{8} - \frac{891\overline{\lambda}^3}{128} - \frac{19551\overline{\lambda}^2}{4096} + \frac{4959\overline{\lambda}}{16384} + \frac{1596155}{3145728}\right)\left(\frac{a}{l}\right)^5, \tag{94}$$

$$c^q_{yx} \sim 1 + \left(\frac{27\overline{\lambda}^2}{32} - \frac{3}{32}\right)\left(\frac{a}{l}\right)^3 - \left(\frac{99\overline{\lambda}^3}{16} - \frac{243\overline{\lambda}^2}{512} - \frac{3\overline{\lambda}}{8} - \frac{9}{256}\right)\left(\frac{a}{l}\right)^4 + \left(\frac{1395\overline{\lambda}^4}{32} - \frac{2025\overline{\lambda}^3}{512} - \frac{39541\overline{\lambda}^2}{8192} - \frac{45\overline{\lambda}}{256} + \frac{977}{4096}\right)\left(\frac{a}{l}\right)^5. \tag{95}$$

Unfortunately, the expansion of s^q_{xz} proposed in (**17**) suffers from several misprint errors (starting with the sign of the term of order a/l). The corrected estimate reads

$$s^q_{xz} \sim 1 - \frac{9}{32}\left(\frac{a}{l}\right) + \left(\frac{9\overline{\lambda}}{16} - \frac{81}{512}\right)\left(\frac{a}{l}\right)^2 + \left(\frac{32451}{40960} + \frac{243\overline{\lambda}}{512} - \frac{81\overline{\lambda}^2}{32}\right)\left(\frac{a}{l}\right)^3 - \left(\frac{18981}{655360} + \frac{26691\overline{\lambda}}{10240} + \frac{1053\overline{\lambda}^2}{512} - \frac{261\overline{\lambda}^3}{16}\right)\left(\frac{a}{l}\right)^4 - \left(\frac{12048973}{10485760} - \frac{28197\overline{\lambda}}{131072} - \frac{71903\overline{\lambda}^2}{4096} - \frac{405\overline{\lambda}^3}{32} + \frac{4005\overline{\lambda}^4}{32}\right)\left(\frac{a}{l}\right)^5. \tag{96}$$

The normalised velocities u_q and ω_q of a sphere freely-suspended in the quadratic shear flow have the following expansions

$$u_q \sim 1 - \frac{5}{8}\left(\frac{a}{l}\right)^3 + \frac{5\overline{\lambda}}{4}\left(\frac{a}{l}\right)^4 + \left(\frac{79}{96} - \frac{45\overline{\lambda}^2}{8}\right)\left(\frac{a}{l}\right)^5, \tag{97}$$

$$\omega_q \sim 1 - \frac{5}{16}\left(\frac{a}{l}\right)^3 + \frac{15\overline{\lambda}}{16}\left(\frac{a}{l}\right)^4 + \left(\frac{1}{4} - \frac{7\overline{\lambda}^2}{2}\right)\left(\frac{a}{l}\right)^5 \tag{98}$$

and the resulting stresslet factor for the freely-suspended sphere behaves as

$$s_{xz}^{q,\text{free}} \sim 1 + \frac{15}{16}\left(\frac{a}{l}\right)^3 - \frac{45\overline{\lambda}}{16}\left(\frac{a}{l}\right)^4 + \left(\frac{161\overline{\lambda}^2}{10} - \frac{79}{64}\right)\left(\frac{a}{l}\right)^5. \tag{99}$$

As for the freely-suspended sphere in a linear shear flow, the results (97)–(99) (not given in (**17**)) show that the freely-suspended sphere rigid-body motion and experienced stresslet are subject to short-range wall-sphere interactions of order $O(\epsilon^3)$ which are sensitive to the wall normalized slip length $\overline{\lambda}$ solely at order $O(\epsilon^4)$ with $\epsilon = a/l \ll 1$.

When comparing the results for the distant sphere freely immersed in a linear or a quadratic shear flow it is noticeable that $\omega_s - \omega_q = O(\epsilon^5)$ and that $s_{xz}^{s,\text{free}} - s_{xz}^{q,\text{free}} = O(\epsilon^5)$!

Finally, comparisons of the derived asymptotic estimates (94)–(99) against the computational predictions (using again the *LU* factorization method detailed in section 5.1) are given in Table **6**.

5.4 *Numerical results for arbitrary sphere location*

This section numerically investigates the case of a sphere located near the slip wall. It should be recalled that (**12**) recently reported accurate results for a sphere translating or rotating parallel with the slip wall in a quiescent liquid or immersed (being either held fixed or freely-suspended) in a linear shear flow except for the stresslet component. However, (**12**) does not deal with the stresslet component for those cases. Therefore, we here confine attention to the quadratic shear flow and also to the stresslet coefficients for a sphere embedded in a linear or quadratic ambient shear flow.

The lubrication problem (for very low $l/a - 1$) was treated in (**12**) on the basis of Thomas' algorithm computations. Recall that the conclusions from (**12**) were that an approximate lubrication formula could be obtained for f_{xx}^t but the cases of f_{yx}^r and c_{yy}^r which involve $\log(l/a - 1)$ were more difficult to tackle and would require a special and involved analytical analysis. In this article, the lubrication regime is not studied in detail. We can simply remark that a singular behaviour of friction factors is expected only when the neighbouring surfaces of the sphere and wall are in relative motion.

5.4.1 Normalised force, torque and rigid-body motion in a quadratic shear flow. Let us start with the force coefficient f_{xx}^q and the torque coefficient c_{yx}^q for a sphere *held fixed* in a quadratic ambient shear flow. These coefficients, admitting asymptotic estimates (94)–(95) for a distant sphere, are plotted versus $l/a \leq 10$ in Fig. 5.

Both quantities slowly tend to unity as the wall-sphere gap increases. That is, sphere-wall interactions are long-range. They also take a finite value as the sphere–wall gap vanishes. Not surprisingly, the normalized force f_{xx}^q is seen to monotonically decrease as l/a or λ/a increases. In addition, for very small sphere–wall and normalised slip length λ/a it is seen that f_{xx}^q may reach twice its value of unity in absence of wall.

In contrast, the torque coefficient exhibits a quite different behaviour. First, c_{yx}^q remains very close to unity (up to 4%) whatever $(l/a, \lambda/a)$. Second, the sensitivity of c_{yx}^q to l/a deeply depends upon the normalised slip length $\overline{\lambda} = \lambda/a \geq 0$. As already pointed out in (**14**) for the no-slip case ($\overline{\lambda} = 0$), it turns out that for $\overline{\lambda} < \overline{\lambda}_c$ (with, from our numerical investigations, a critical slip length $\overline{\lambda}_c < 0.1$) the coefficient c_{yx}^q first decreases and then increases with increasing l/a, thereby admitting a minimum. Such a minimum is located very close to the wall, in practice at $l \sim 1.2a$ (for instance, see (**14**), for $\overline{\lambda} = 0$ the minimum takes place at $l = 1.18a$). For $\overline{\lambda} > \overline{\lambda}_c$, c_{yx}^q first increases and then decreases with increasing l/a, therefore admitting a maximum located around $l = 2a$.

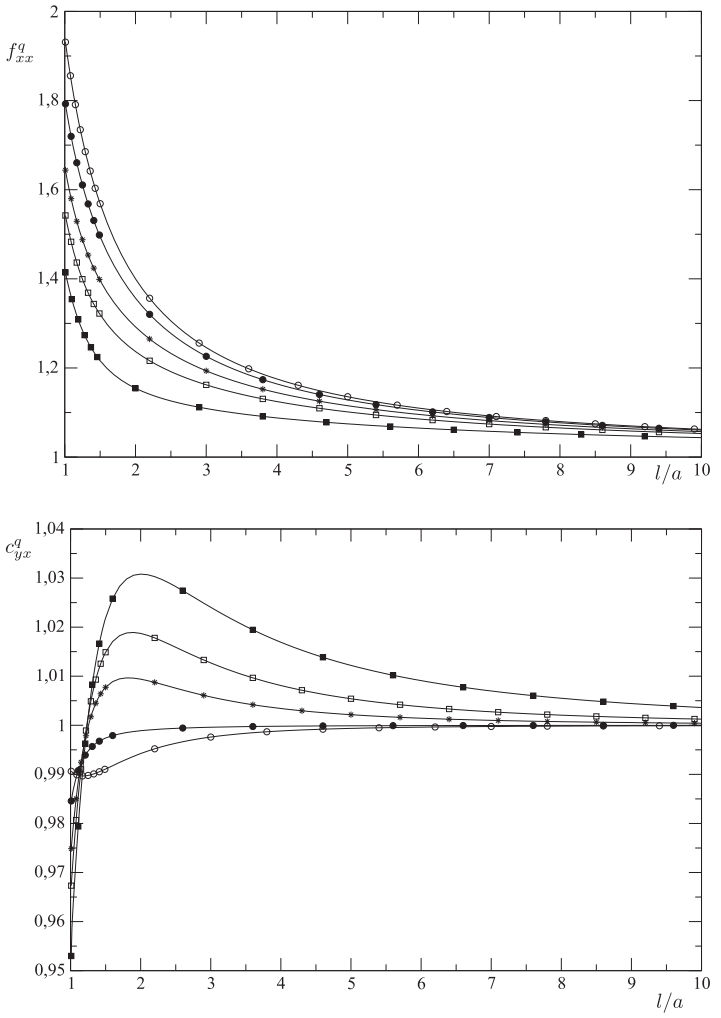

Fig. 5 Force and torque friction coefficients f^q_{xx} and c^q_{yx} for a sphere *held fixed* in a quadratic shear flow above a slip wall versus l/a and for $\lambda/a = 0$ ($\circ$), $\lambda/a = 0.3$ ($\bullet$), $\lambda/a = 1$ ($*$), $\lambda/a = 2$ ($\square$) and $\lambda/a = 5$ ($\blacksquare$)

Both normalised translational velocity u_q and angular velocity ω_q of a freely-suspended sphere in a quadratic shear flow are displayed in Fig. 6.

As revealed by the asymptotic estimates (97)–(98), these quantities tend to unity very fast as a/l vanishes. We therefore plot them only in the range $1 < l/a \leq 4$. It is observed that variations of u_q with $\overline{\lambda}$ are significant whereas those of ω_q with $\overline{\lambda}$ are small. Moreover, wall-sphere interactions slow down ($u_q < 1$ and $\omega_q < 1$) the sphere translational and rotational motions whatever (l/a, λ/a). Moreover, for a given sphere location l/a, increasing the wall slip length also increases the sphere translational velocity u_q while the sphere rotation may either increase or decrease depending upon

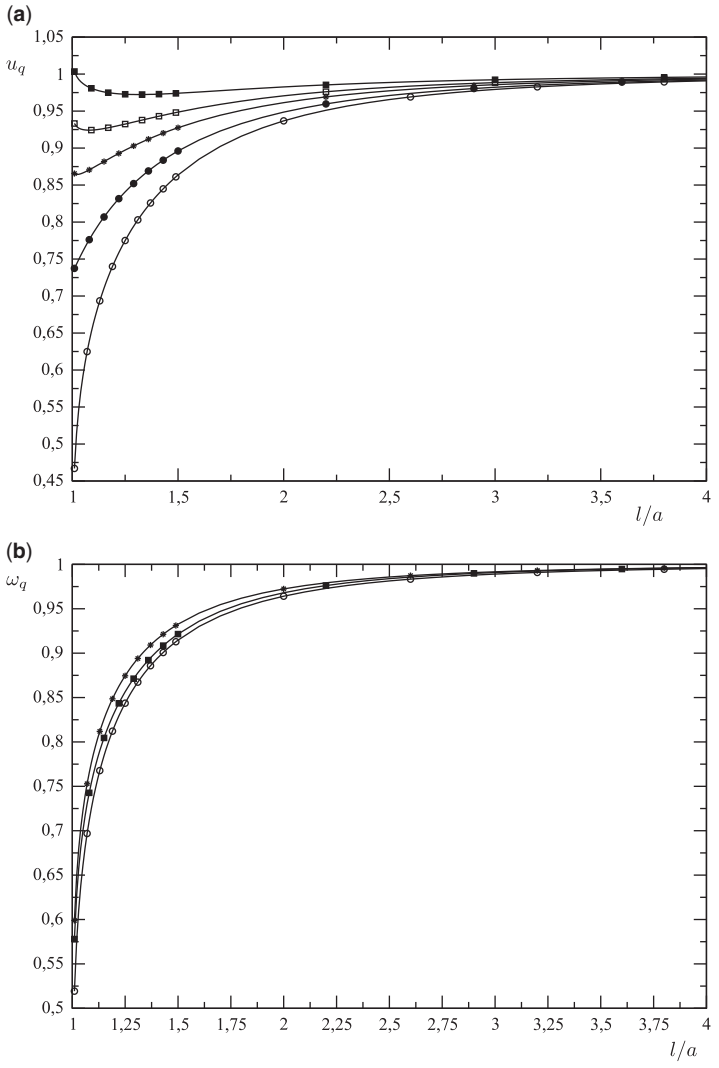

Fig. 6 Normalised translational velocity u_q and angular velocity ω_q for a sphere *freely suspended* in a quadratic shear flow above a slip wall versus l/a and for $\lambda/a = 0$ ($\circ$), $\lambda/a = 0.3$ ($\bullet$), $\lambda/a = 1$ ($*$), $\lambda/a = 2$ ($\square$) and $\lambda/a = 5$ ($\blacksquare$)

the value of $\overline{\lambda}$ (in fact our computations reveal that ω_q goes through a maximum for $\overline{\lambda} \sim 0.5$). On the other hand for a prescribed normalised slip length $\overline{\lambda}$ it is observed that the sphere angular velocity ω_q decreases as the sphere approaches the slip wall as also does u_q except for a sphere sufficiently close to a slipping enough wall (see the curves for $\overline{\lambda} \geq 0.3$ in Fig. 6a).

Finally, we provide in Table **7** the computed quantities f_{xx}^q, c_{yx}^q, u_q and ω_q (using again the *LU* factorisation algorithm with $N = 12000$) for several values of $(l/a, \lambda/a)$.

Table 7 Computed normalised quantities f^q_{xx}, c^q_{yx}, u_q and ω_q for different sphere locations l/a and wall slip lengths λ/a using the LU factorisation algorithm with $N = 12000$

l/a	λ/a	f^q_{xx}	c^q_{yx}	u_q	ω_q
1.005	0	1.936889	0.990700	0.427204	0.473260
1.01	0	1.931038	0.990632	0.467002	0.519313
1.1	0	1.836197	0.989853	0.663247	0.737156
2	0	1.399981	0.994236	0.936735	0.964149
5	0	1.135383	0.999367	0.995220	0.997561
10	0	1.062357	0.999912	0.999383	0.999689
1.005	0.3	1.797790	0.984127	0.735015	0.569063
1.01	0.0	1.792630	0.984578	0.737422	0.610671
1.1	0.3	1.711689	0.990333	0.785635	0.794186
2	0.3	1.356702	0.998891	0.948566	0.971078
5	0.3	1.128282	0.999894	0.995672	0.997858
10	0.3	1.060606	0.999984	0.999415	0.999712
1.005	1	1.648368	0.974016	0.867812	0.556745
1.01	1	1.643818	0.974867	0.865601	0.598963
1.1	1	1.572887	0.987409	0.873677	0.786536
2	1	1.292192	1.009399	0.961394	0.972373
5	1	1.115306	1.002156	0.996315	0.998105
10	1	1.057084	1.000423	0.999471	0.999742
1.005	2	1.546373	0.966244	0.937303	0.546933
1.01	2	1.542164	0.967327	0.933235	0.588944
1.1	2	1.476612	0.983918	0.924460	0.776407
2	2	1.236876	1.018721	0.970606	0.971020
5	2	1.101440	1.005407	0.996866	0.998171
10	2	1.052920	1.001254	0.999525	0.999760
1.005	5	1.418068	0.955043	1.009252	0.536368
1.01	5	1.414224	0.956375	1.003528	0.577958
1.1	5	1.354342	0.977386	0.979705	0.764144
2	5	1.154433	1.030813	0.982599	0.968018
5	5	1.074621	1.012203	0.997724	0.998091
10	5	1.043688	1.003622	0.999622	0.999768

5.4.2 Stresslet components in linear and quadratic shear flows. As previously mentioned, the stresslet factors $s^{s,\text{free}}_{xz}$ and $s^{q,\text{free}}_{xz}$ for a freely moving sphere would be of the utmost importance in evaluating the viscosity of a dilute suspension of solid spheres embedded in a pure (k_s) or a quadratic (k_q) shear flow close to a slipping wall.

For completion and comparison purposes, we also plot in Fig. 7 the normalised stresslets s^s_{xz} and s^q_{xz} obtained when the sphere is *held fixed* in the ambient linear and quadratic shear flows.

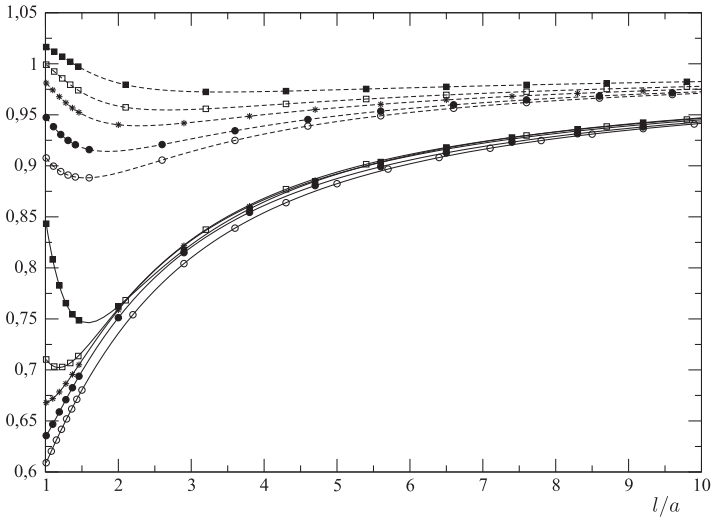

Fig. 7 Normalised stresslets s^s_{xz} (dashed lines) and s^q_{xz} (solid lines) for a sphere *held fixed* in linear and quadratic shear flows above a slip wall versus l/a and for $\lambda/a = 0$ (○), $\lambda/a = 0.3$ (●), $\lambda/a = 1$ (∗), $\lambda/a = 2$ (□) and $\lambda/a = 5$ (■)

These coefficients remain bounded and $s^s_{xz} > s^q_{xz}$ whatever $(l/a, \lambda/a)$. Clearly, both s^s_{xz} and s^q_{xz} slowly decay to unity as l/a increases (recall the predictions (90) and (96)). At a given sphere location l/a both quantities increase with $\overline{\lambda}$. Note that $|s^s_{xz} - 1|$ is at most of order 10% and, at given $\overline{\lambda}$, it appears that s^s_{xz} first decreases and then increases as l/a increases, the minimum being around $l = 2a$. The coefficient s^q_{xz} exhibits a similar behaviour for $\overline{\lambda}$ large enough (see the curves for $\overline{\lambda} \geq 1$ in Fig. 7) but monotonically increases with l/a for a weakly slipping wall.

The normalised stresslets $s^{s,free}_{xz}$ and $s^{q,free}_{xz}$ for a *freely-suspended* sphere are plotted in Fig. 8. These coefficients follow the same behaviour as for the force coefficient f^q_{xx} (see the previous comments about Fig. 5) except that a faster decay toward unity is observed for a distant sphere (as shown by (93) and (99)).

Comparing Fig. 8a and b reveals that the values of $s^{s,free}_{xz}$ and $s^{q,free}_{xz}$ are close, a property which was not true for the case of a sphere *held fixed* in a shear flow (as seen in Fig. 7)! This has been already pointed out at the end of section 5.2, for a distant sphere. As shown in Fig. 9, the difference $s^{s,free}_{xz} - s^{q,free}_{xz}$ is actually positive and of small value even when the sphere is close to the wall.

It is straightforward to show that a Poiseuille flow between two slip planes, with equal slip length λ, located at $z = 0$ and $z = h > 0$ has the following velocity

$$\mathbf{w} = k_s[z + \lambda - z^2/h]\mathbf{e}_x, \quad k_s = -\frac{h}{2\mu}\frac{dp}{dx} \tag{100}$$

with dp/dx the imposed uniform pressure gradient. If the sphere is close to the lower $z = 0$ wall, i. e. if $l \ll h/2$ we can ignore the interactions with the upper wall and using the relationship $k_q = -k_s/h$ obtain the stresslet component S^{free}_{xz}, with associated normalised coefficient s^{free}_{xz}, experienced by the

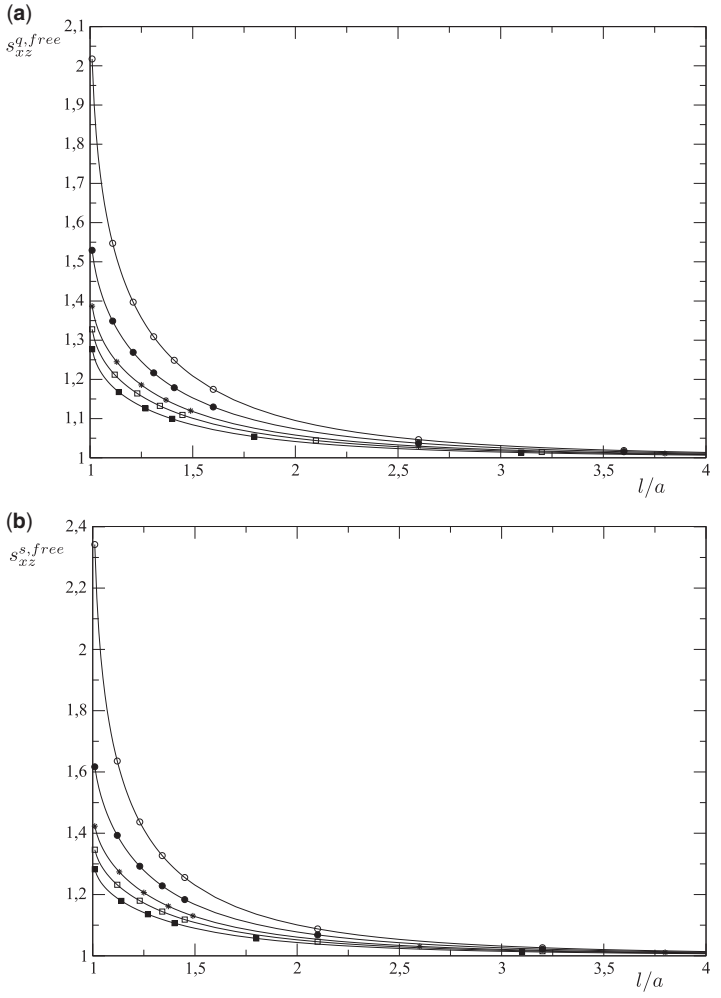

Fig. 8 Normalised stresslets $s_{xz}^{q,free}$ and $s_{xz}^{s,free}$ for a sphere *freely suspended* in quadratic and linear ambient shear flows above a slip wall versus l/a and for $\lambda/a = 0$ (○), $\lambda/a = 0.3$ (●), $\lambda/a = 1$ (∗), $\lambda/a = 2$ (□) and $\lambda/a = 5$ (■)

sphere as

$$s_{xz}^{free} = \frac{S_{xz}^{free}}{\frac{10}{3}\pi\mu a^3 k_s} = s_{xz}^{s,free} - (\frac{2l}{h}) s_{xz}^{q,free}. \tag{101}$$

Since $2l/h < 1$ and all quantities $s_{xz}^{s,free}$, $s_{xz}^{q,free}$ and $s_{xz}^{s,free} - s_{xz}^{q,free}$ are positive it then turns out that $s_{xz}^{free} > 0$ whatever λ/a.

We close this subsection by listing in Table **8** (for the same pairs $(l/a, \lambda/a)$ as the ones selected in Table **7**) the computed values of the previously plotted stresslet coefficients and also the two

Table 8 Computed normalised stresslet components for different sphere locations l/a and wall slip lengths λ/a using the LU factorisation algorithm with $N = 12000$

l/a	λ/a	s^r_{xz}	s^t_{xz}	s^q_{xz}	$s^{q,free}_{xz}$	s^s_{xz}	$s^{s,free}_{xz}$
1.005	0	0.582814	1.872330	0.908248	2.118734	0.608212	2.495611
1.01	0	0.491603	1.562291	0.907759	2.017436	0.609035	2.342179
1.1	0	0.205187	0.635760	0.900382	1.568960	0.623518	1.692766
2	0	0.024173	0.099109	0.893126	1.095137	0.735885	1.100859
5	0	0.001627	0.013732	0.943389	1.007168	0.882492	1.007239
10	0	0.000207	0.003288	0.971071	1.000926	0.941584	1.000928
1.005	0.3	0.526546	0.383801	0.947835	1.556877	0.635069	1.645528
1.01	0.0	0.450447	0.376142	0.947375	1.529466	0.635627	1.616888
1.1	0.3	0.185817	0.289837	0.939165	1.359511	0.646801	1.418512
2	0.3	0.019946	0.076615	0.914513	1.073660	0.751195	1.077808
5	0.3	0.001431	0.012348	0.948897	1.006244	0.887467	1.006303
10	0.3	0.000192	0.003109	0.972630	1.000856	0.943070	1.000858
1.005	1	0.522939	0.157755	0.981524	1.408248	0.667850	1.443191
1.01	1	0.450642	0.155929	0.981152	1.386859	0.667966	1.423013
1.1	1	0.200241	0.135709	0.974312	1.265775	0.671762	1.297292
2	1	0.020001	0.053497	0.940196	1.057990	0.758845	1.061055
5	1	0.001274	0.010378	0.956904	1.005197	0.892195	1.005245
10	1	0.000172	0.002803	0.975297	1.000753	0.945107	1.000755
1.005	2	0.521673	0.080525	0.999446	1.346986	0.710754	1.363678
1.01	2	0.450389	0.079863	0.999151	1.327776	0.710255	1.346255
1.1	2	0.206455	0.073744	0.993663	1.224012	0.704074	1.244462
2	2	0.021391	0.038309	0.958553	1.049754	0.760004	1.052249
5	2	0.001240	0.008707	0.963808	1.004502	0.893844	1.004542
10	2	0.000161	0.002504	0.977920	1.000668	0.946442	1.000670
1.005	5	0.520373	0.021976	1.016615	1.294497	0.845510	1.297608
1.01	5	0.449930	0.021940	1.016420	1.277001	0.843264	1.282273
1.1	5	0.211167	0.023274	1.012726	1.186744	0.808260	1.198256
2	5	0.023606	0.020732	0.911560	1.041446	0.762333	1.043375
5	5	0.001305	0.006155	0.974508	1.003681	0.891822	1.003713
10	5	0.000155	0.001976	0.982570	1.000550	0.947056	1.000551

additional coefficients s^r_{xz} and s^t_{xz} for the sphere rotating and translating parallel with the slip wall in a quiescent liquid.

6. Conclusions

A general solution in bipolar coordinates has been obtained for a sphere either held fixed or freely-suspended near a slip wall in an ambient modulated rotational flow and linear or quadratic shear

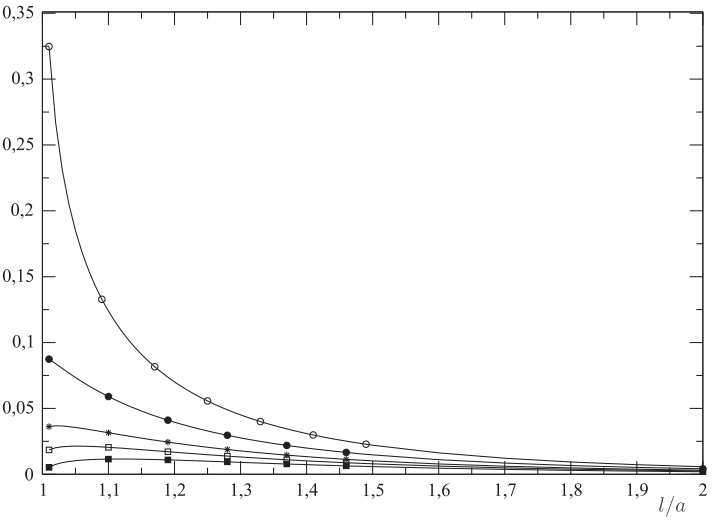

Fig. 9 Quantity $s_{xz}^{s,free} - s_{xz}^{q,free}$ versus l/a and for $\lambda/a = 0$ (○), $\lambda/a = 0.3$ (●), $\lambda/a = 1$ (∗), $\lambda/a = 2$ (□) and $\lambda/a = 5$ (■)

flows. The solution for the modulated shear flow is new. The presented results also complement earlier works for the linear (**10**–**12**) and quadratic (**17**, **18**) shear flows. The associated (either friction or mobility) coefficients for several quantities (force, torque, translational velocity, angular velocity, non-zero stresslet component) have been obtained for different sphere locations and wall slip lengths. For the linear (**10**– **12**) and quadratic (**17**, **18**) shear flows, the novelty here is the evaluation of the stresslet.

The bipolar coordinates method is quite appropriate to provide very accurate results, even at small wall–sphere gaps. To reach this goal, the boundary conditions on the wall and on the sphere boundary have first to be carefully cast into relationships between unknown coefficients, reducing the number of equations from 7 (like in (**10**)) to 4 (like in **11**, **12**) (see section 4.1 for details). Second, the resulting infinite linear system has to be adequately truncated and inverted in order to reach the expected accuracy level of resolution (see section 5.1 and also Table **5**). Methods to reach this goal depend upon the flow field. The classical implicit method inverting a large matrix may be used for all flow fields. Methods using less computer memory are explicit ones: (i) for an axisymmetric flow field, the one pioneered in (**23**) (see section 3.3); (ii) for a symmetric flow field, the so-called Thomas' algorithm detailed in (**17**) (see section 5.1). The merits and drawbacks of each method are discussed in the relevant subsections sections 3.3 and 5.1.

Two types of results are provided: numerical results valid for any sphere location and asymptotic ones valid for a distant sphere. Comprehensive numerical results are provided by figures and tables for all friction and mobility coefficients in a large range of normalised slip length and sphere-to-wall distances. Asymptotic expansions for the coefficients are derived from the general solution in bispherical coordinates. These asymptotic expansions are new for the linear and modulated shear flows and complement results (**17**, **18**) for the quadratic shear flow. It is shown that the numerical and asymptotic results match for a distant sphere. Moreover, the asymptotic analysis

reveals that depending upon the addressed friction coefficient either long-range ($O(a/l)$) or short-range ($O(a^3/l^3)$) weak interactions occur between the slip wall and a distant sphere. With a few terms only, these asymptotic expansions provide handy formulae in view of practical applications.

A no-slip sphere was considered in this article. The interesting cases of a slip sphere translating normal to a slip wall and *held fixed* in a *linear* shear flow near a slip wall have been handled in (**7**) (using again bipolar coordinates) and in (**33**) (using the boundary integral approach), respectively. In a similar way, it should be possible to extend the present analysis, still using the bipolar coordinates, to a slip sphere either held fixed or freely suspended in a quadratic shear.

Even for the no-slip particle, most of the works available in the literature are, like the present one, restricted to the case of a spherical particle. Since non-spherical particles are encountered in practice it would be useful in future to also deal with a solid arbitrary-shaped particle so as to quantity shape effects. Clearly, those problems are not solvable with the bipolar coordinates technique which, by essence, restricts the analysis to a sphere. One can think about using a boundary integral technique while exploiting the present results for a sphere to benchmark the boundary procedure. Hence, we are currently developing a boundary approach with a relevant Green tensor for a slip wall so that only the body surface has to be meshed (it thus differs from the technique implemented in (**33**)). This already provided a confirmation of the present results for the modulated rotational flow (see comments in section 3.3). However, since it requires additional efforts, its presentation and results for a non-spherical solid particle immersed in a linear or a quadratic shear flow are postponed to a future work.

References

1. H. A. Stone, A. D. Stroock and A. Adjari, Slippage of liquids over lyophobic solid surfaces, *Annu. Rev. Fluid Mech.* **36** (2004) 381–411.

2. C. L. M. H. Navier, Mémoire sur les lois du mouvement des fluides, *Mémoires de l'Acad. des Sciences de l'Institut de France* **6** (1823) 389–416.

3. N. V. Churaev, V. D. Sobolev and A. N. Somov, Slippage of liquids over lyophobic solid surfaces, *J. Colloid Int. Sci.* **97** (1984) 574–581.

4. J. Baudry, E. Charlaix, A. Tonck and D. Mazuyer, Experimental evidence for a large slip effect at a nonwetting fluid-solid interface, *Langmuir* **17** (2001) 5232–5236.

5. D. Lumma, A. Best, A. Gansen, F. Feuillebois, J. O. Rädler and O. I. Vinogradova, Flow profile near a wall measured by double-focus fluorescence cross correlation, *Phys. Rev. E* **67** (2003), doi: 10.1103/PhysRevE.67.056313.

6. O. I. Vinogradova, K. Koynov, A. Best and F. Feuillebois, Direct measurements of hydrophobic slippage using double-focus fluorescence cross-correlation, *Phys. Rev. Lett.* **102** (2009), doi: 10.1103/PhysRevLett.102.118302.

7. S. L. Goren, The hydrodynamic force resisting the approach of a sphere to a plane in slip flow, *J. Colloid Interface Sci.* **44** (1973) 356–360.

8. L. M. Hocking, The effect of slip on the motion of a sphere close to a wall and of two adjacent spheres, *J. of Engineering Math.* **7** (1973) 207–221.

9. M. E. O'Neill and B. S. Bhatt, Slow motion of a solid sphere in the presence of a naturally permeable surface, *Q. J. Mech. Appl. Math.* **44** (1991) 91–104.

10. A. M. J. Davis, M. T. Kezirian and H. Brenner, On the Stokes-Einstein model of surface diffusion along solid surfaces: slip boundary conditions, *J. Colloid Interface Sci.*, **1065** (1994) 129–140.

11. F. Feuillebois, H. Loussaief and L. Pasol, Particles in creeping flow near a slip wall, *App. Math. Tech. Nat. Sci.* **1186** (2009) 3–14.
12. H. Loussaief, L. Pasol and F. Feuillebois, Motion of a spherical particle in a viscous fluid along a slip wall, *Q. J. Mech. Appl. Math.* **68** (2015) 115–144.
13. S. L. Goren and M. E. O'Neill, On the hydrodynamic resistance to a particle of a dilute suspension when in the neighborhood of a large obstacle, *Chem. Engng. Sci.* **26** (1971) 325–338.
14. L. Pasol, A. Sellier and F. Feuillebois, A sphere in a second degree polynomial creeping flow parallel to a wall, *Q. J. Mech. Appl. Math.* **59** (2006) 587–614.
15. L. Pasol, A. Sellier and F. Feuillebois, Creeping flow around a solid sphere in the vicinity of a plane solid wall, *Theoretical Methods for Micro Scale Viscous Flows* (eds Feuillebois, F. and A. Sellier; Transworld Research Network, Kerala 2009) 105–126.
16. M. Chaoui and F. Feuillebois, Creeping flow around a sphere in a shear flow close to a wall, *Quart. J. Mech. Applied Math.* **56** (2003) 381–410.
17. F. Feuillebois, N. Ghalya, A. Sellier and L. Elasmi, Motion of particles in a parabolic flow near a slip wall, *App. Math. Tech. Nat. Sci.* **1404** (2011) 340–351.
18. F. Feuillebois, N. Ghalya, A. Sellier and L. Elasmi, Influence of wall slip in dilute suspensions, *J. of Physics : Conference Series* **392** (2012) 1–19.
19. J. Happel and H. Brenner, *Low Reynolds Number Hydrodynamics* Noordhoff, Leyden (1973).
20. H. Brenner, The slow motion of a sphere through a viscous fluid towards a plane surface, *Chem. Eng. Sci.* **16** (1961) 242–251.
21. A. D. Maude, End effects in a falling-sphere viscometer, *Br. J. Appl. Phys.* **12** (1961) 293–295.
22. G. B. Jeffery, On the steady rotation of a solid of revolution in a viscous fluid, *Proc. London Math. Soc.* **14** (1915) 327–338.
23. A. M. Davis and M. E. O'Neill, The slow rotation of a sphere submerged in a fluid with a surfactant surface layer, *Int. Jl Multiphase Flow* **5** (1979) 413–425.
24. H. Faxen, Der Widerstand gegen die Bewegung einer starren Kugel in einer zaehen Fluessigkeit, die zwischen zwei parallelen ebenen Waenden eigeschlossen ist, *Annalen des Physik* **IV** (1922) 89–119.
25. W. R. Dean and M. E. O'Neill, A slow rotation of viscous liquid caused by the rotation of a solid sphere, *Mathematika* **10** (1963) 13–24.
26. M. E. O'Neill, A slow motion of viscous liquid caused by a slowly moving solid sphere, *Mathematika* **11** (1964) 67–74.
27. M. E. O'Neill, A slow motion of viscous liquid caused by a slowly moving solid sphere: an addendum. *Mathematika* **14** (1967) 170–172.
28. G. K. Batchelor, The stress system in a suspension of force-free particles, *J. Fluid Mech.* **41** (1970) 545–570.
29. G. K. Batchelor and J. T. Green, The hydrodynamic interaction of two small freely-moving spheres in a linear flow field, *J. Fluid Mech.* **56** (1972) 375–400.
30. G. K. Batchelor and J. T. Green, The determination of the bulk stress in a suspension of spherical particles to order c^2, *J. Fluid Mech.* **56** (1972) 401–427.
31. H. Tözeren and R. Skalak, Stress in a suspension near rigid boundaries, *J. Fluid Mech.* **82** (1983) 289–307.
32. F. Feuillebois and J. Bławdziewicz, Calculation of an effective slip in settling suspension at a vertical wall, *Fluid Mech. Res.* **22** (1995) 66–67.
33. H. Luo and C. Pozrikidis, Effect of surface slip on Stokes flow past a spherical particle in infinite fluid and near a plane wall, *J. Eng. Math.* **62** (2008) 1–21.

APPENDIX A

Boundary conditions on the sphere for the quadratic shear flow

This Appendix briefly displays the steps employed in deriving the relations (45)–(47) from the boundary conditions (43) on the sphere's surface $S(\xi = \alpha)$ for the quadratic shear flow. Exploiting (33)–(34), the relations (43) become

$$U_2 = \frac{\rho}{z} W_1, \;\; U_0 = \frac{\rho}{z} W_1 - 2z^2 \quad \text{and} \quad Q_1 = -\frac{2c}{z} W_1 \quad \text{for } \xi = \alpha. \tag{A.1}$$

Recalling (12), (35) and (38) the first relation $zU_2 = \rho W_1$ immediately gives

$$\sinh\alpha \sum_{n\geq 2} [F_n \cosh(\gamma_n \xi) + G_n \sinh(\gamma_n \xi)] P_n''(t) = \sum_{n\geq 1} A_n \sinh(\gamma_n \xi) P_n'(t). \tag{A.2}$$

According to (**25**) one has the useful identities

$$(2n+1)P_n'(t) = P_{n+1}''(t) - P_{n-1}''(t) \quad \text{for } n \geq 1, \tag{A.3}$$

$$(2n+1)(1-t^2)P_n'(t) = n(n+1)[P_{n-1}(t) - P_{n+1}(t)] \quad \text{for } n \geq 1, \tag{A.4}$$

$$(2n+1)tP_n'(t) = (n+1)P_{n-1}'(t) + nP_{n+1}'(t) \quad \text{for } n \geq 1, \tag{A.5}$$

$$\frac{\sinh^2\alpha}{(\cosh\alpha - t)^{5/2}} = \frac{4\sqrt{2}}{3} \sum_{n\geq 0} \gamma_n [\gamma_n + \coth\alpha] \mathrm{e}^{-\gamma_n \alpha} P_n(t). \tag{A.6}$$

Injecting (A.3) in (A.2) then establishes (47). For the quadratic shear flow $M = 2$. Using (A.4)–(A.5) then shows that it also easily follows that

$$\frac{z^2}{c^2} = \frac{4\sqrt{2}}{3} (\cosh\alpha - t)^{1/2} \sum_{n\geq 0} \gamma_n [\gamma_n + \coth\alpha] \mathrm{e}^{-\gamma_n \alpha} P_n(t), \tag{A.7}$$

$$\frac{\rho W_1}{zc^2} = \frac{(\cosh\alpha - t)^{1/2}}{\sinh\alpha} \sum_{n\geq 1} [\frac{n(n+1)}{2n+1}] A_n \sinh(\gamma_n \xi)[P_{n-1}(t) - P_{n+1}(t)]. \tag{A.8}$$

Combining (A.7)–(A.8) with (37) for $M = 2$ (quadratic shear flow) accordingly makes it possible to cast the second relation (A.1) in (46) with the definition (48) of $K_n^{(2)}$. Finally, appealing to (35)–(36) in enforcing the last relation (A.1) gives

$$\sinh\alpha \sum_{n\geq 1} [B_n \cosh(\gamma_n \alpha) + C_n \sinh(\gamma_n \alpha)] P_n'(t) = 2 \sum_{n\geq 1} A_n \sinh(\gamma_n \alpha)(t - \cosh\alpha) P_n'(t). \tag{A.9}$$

Using (A.5) then produces (45) with, as defined in (48), $f_n^{(2)} = 0$.

APPENDIX B

Frictions coefficients

The friction coefficients f^t_{xx}, c^t_{yx}, f^r_{xy}, f^s_{xx}, c^s_{yx} and also s^t_{xz}, s^r_{xz} and s^s_{xz} defined by (62)–(64) read

$$f^t_{xx} = \frac{\sqrt{2}\sinh\alpha}{6} F(C^s_n; E^s_n),\ c^t_{yx} = \frac{\sqrt{2}\sinh^2\alpha}{4} T(A^s_n; E^s_n), \tag{B.1}$$

$$f^s_{xx} = \frac{\sqrt{2}\sinh^2\alpha}{6k_s(l+\lambda)} F(C^t_n; E^t_n),\ c^s_{yx} = \frac{\sqrt{2}\sinh^2\alpha}{2} T(A^t_n; E^t_n), \tag{B.2}$$

$$f^r_{xy} = -\frac{\sqrt{2}\sinh^2\alpha}{6} F(C^r_n; E^r_n),\ s^r_{yx} = \frac{\sqrt{2}\sinh^3\alpha}{6} S(B^r_n; C^r_n; E^r_n), \tag{B.3}$$

$$s^t_{yx} = \frac{\sqrt{2}\sinh^2\alpha}{6} S(B^t_n; C^t_n; E^r_n),\ s^s_{yx} = \frac{3\sqrt{2}\sinh^3\alpha}{10} S(B^s_n; C^s_n; E^s_n). \tag{B.4}$$